

COMPARISON OF TREATMENT PLANS CALCULATED USING RAY TRACING
AND MONTE CARLO ALGORITHMS FOR LUNG CANCER PATIENTS HAVING
UNDERGONE RADIOTHERAPY WITH CYBERKNIFE

by

Andreea Pennington

A Thesis Submitted to the Faculty of
The Charles E. Schmidt College of Science
In Partial Fulfillment of the Requirements for the Degree of
Professional Science Master

Florida Atlantic University

Boca Raton, Florida

December 2014

Copyright 2014 by Andreea Pennington

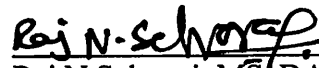
COMPARISON OF TREATMENT PLANS CALCULATED USING RAY TRACING
AND MONTE CARLO ALGORITHMS FOR LUNG CANCER PATIENTS HAVING
UNDERGONE RADIOTHERAPY WITH CYBERKNIFE

by

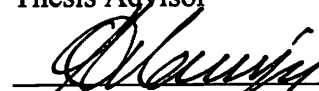
Andreea Pennington

This thesis was prepared under the direction of the candidate's thesis advisor, Raj N Selvaraj, MS, DABR, DABMP, Research Affiliate Associate Professor, Department of Physics, and has been approved by the members of her supervisory committee. It was submitted to the faculty of the Charles E. Schmidt College of Science and was accepted in partial fulfillment of the requirements for the degree of Professional Science Master.

SUPERVISORY COMMITTEE:



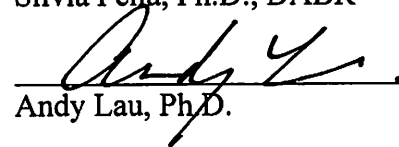
Raj N Selvaraj, MS, DABR, DABMP
Thesis Advisor



Theodora Leventouri, Ph.D.
Thesis Co-Advisor



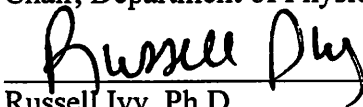
Silvia Pella, Ph.D., DABR



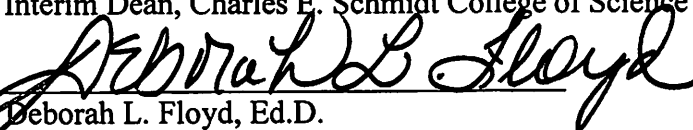
Andy Lau, Ph.D.



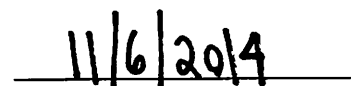
Warner Miller, Ph.D.
Chair, Department of Physics



Russell Ivy, Ph.D.
Interim Dean, Charles E. Schmidt College of Science



Deborah L. Floyd, Ed.D.
Interim Dean, Graduate College


Date

ACKNOWLEDGEMENTS

I would like to express my special appreciation and thanks to my advisor Raj Selvaraj, MS, DABR, DABMP, Director of Medical Physics, Broward Health Operations for 21st Century Oncology, and Research Affiliate Associate Professor at FAU. I would like to thank him for encouraging my research and guiding me to design and complete this project.

I would especially like to thank Dr. Theodora Leventouri, Thesis Co-Advisor, Professor of Physics, and Director of the Medical Physics program. Her advice throughout my matriculation at FAU and, in particular, during the writing phases of this project has been priceless.

I would like also to thank Dr. Silvia Pella, DABR, Medical Physicist for 21st Century Oncology, and Adjunct Research Affiliate Associate Professor at FAU and Dr. Andy Lau, Associate Professor of Physics at FAU for serving as my committee members.

Special thanks, as well, to my lab colleagues Steven Kirkpatrick, MS, DABR, DABMP and Silvana Oliveira, MS, DABR, DABFM as well as all of the physicians, therapists, nurses and other staff at the cancer center at Broward Health North, 21st Century Oncology. All have been there to support and advise me throughout my career and provide morale support during the work on this project.

ABSTRACT

Author: Andreea Pennington

Title: Comparison of Treatment Plans Calculated Using Ray Tracing and Monte Carlo Algorithms for Lung Cancer Patients Having Undergone Radiotherapy with Cyberknife

Institution: Florida Atlantic University

Thesis Advisor: Raj N Selvaraj, MS, DABR, DABMP

Degree: Professional Science Master

Year: 2014

The purpose of this research is to determine the feasibility of introducing the Monte Carlo (MC) dose calculation algorithm into the clinical practice. Unlike the Ray Tracing (RT) algorithm, the MC algorithm is not affected by the tissue inhomogeneities, which are significant inside the chest cavity. A retrospective study was completed for 102 plans calculated using both the RT and MC algorithms. The D95 of the PTV was 26% lower for the MC calculation. The first parameter of conformality, as defined as the ratio of the Prescription Isodose Volume to the PTV Volume was on average 1.27 for RT and 0.67 for MC. The results confirm that the RT algorithm significantly overestimates the dosages delivered confirming previous analyses. Correlations indicate that these overestimates are largest for small PTV and/or when the ratio of the volume of lung tissue to the PTV approaches 1.

DEDICATION

This manuscript is dedicated to my family, particularly to my understanding and loving husband, Jeremy, who has encouraged and supported me through these years of research, and to my son, Jeremy Jr., and daughter, Maria, who are the joys of my life.

COMPARISON OF TREATMENT PLANS CALCULATED USING RAY TRACING AND MONTE CARLO ALGORITHMS FOR LUNG CANCER PATIENTS HAVING UNDERGONE RADIOTHERAPY WITH CYBERKNIFE

| | |
|--|-----------|
| LIST OF TABLES | ix |
| LIST OF FIGURES | x |
| I. INTRODUCTION | 1 |
| A. Purpose: Correlating RT and MC Dose Calculations | 2 |
| B. Lung Cancer | 3 |
| C. Radiation Therapies | 5 |
| 1. Brachytherapy | 8 |
| 2. External Beam Radiation Therapy for Lung Cancer | 10 |
| D. Treatment Planning for Cyberknife | 23 |
| 1. Ray-Tracing Algorithm..... | 26 |
| 2. Monte-Carlo Algorithm | 27 |
| II. METHODS | 31 |
| A. Treatment plan selection | 31 |
| B. RT treatment plans | 31 |
| C. MC treatment plans..... | 33 |
| D. Data Analysis | 34 |
| E. Statistics..... | 37 |

| | |
|--|-----------|
| III. RESULTS | 38 |
| A. Dose parameters | 38 |
| B. Dose parameters versus APR | 48 |
| C. RTOG Protocol Criteria | 52 |
| D. Organs at Risk (OAR) | 57 |
| IV. CONCLUSIONS | 60 |
| APPENDICES..... | 62 |
| A. Appendix 1: IRB Letter | 63 |
| REFERENCES..... | 64 |

LIST OF TABLES

| | |
|--|----|
| Table I: Dose Limits for OARs in the Thorax. | 7 |
| Table II: Calculation Times using Different Options of the MC Algorithm in CyberKnife. | 25 |
| Table III: RTOG Standard Protocol Values | 36 |
| Table IV: T-test results for GTV and PTV Dose Parameters..... | 39 |
| Table V. Correlations for Dose Parameters | 46 |
| Table VI. Spearmen Rank Correlations for Select Dose Parameters..... | 47 |
| Table VII. Kruskal-Wallis Test Statistics for Selected Dose Parameters | 47 |
| Table VIII. RTOG Protocol Values: T-test and Correlations..... | 53 |
| Table IX. OAR Data Details | 58 |

LIST OF FIGURES

| | |
|---|----|
| Figure 1: A study of signaling pathways involved in lung cancer. | 4 |
| Figure 2: Schematic diagram of lung cancer metastases. | 6 |
| Figure 3: 3DCRT of a tumor (denoted by red) in the left upper lobe. | 12 |
| Figure 4: Comparison between IMRT and conventional radiotherapy. | 14 |
| Figure 5: Side view of the axes of movement and volume covered by Cyberknife's robotic arm. | 19 |
| Figure 6: Color coded lung atlas showing different regions. | 22 |
| Figure 7: Schematic based on ICRU report 62 with the GTV, clinical target volume, internal target volume, and PTV as well as an OAR..... | 32 |
| Figure 8: CT-Scan showing differences in PTV between RT and MC calculated plans..... | 34 |
| Figure 9: Graphical DVH (top) comparison between the RT and MC calculations and tabular DVH (bottom) for the historic RT calculated plan. | 35 |
| Figure 10: D99 versus GTV | 42 |
| Figure 11: Dmean versus GTV | 42 |
| Figure 12: D95 versus GTV | 43 |

| | |
|--|----|
| Figure 13: D1 versus GTV | 43 |
| Figure 14: D99 versus PTV..... | 44 |
| Figure 15: Dmean versus PTV..... | 44 |
| Figure 16: D95 versus PTV..... | 45 |
| Figure 17: D1 versus PTV | 45 |
| Figure 18: D99 versus APR | 49 |
| Figure 19: Dmean versus APR | 50 |
| Figure 20: D95 versus APR | 50 |
| Figure 21: D1 versus APR..... | 51 |
| Figure 22: RTOG Protocols: CI versus PTV | 54 |
| Figure 23: RTOG Protocols: R50% versus PTV | 54 |
| Figure 24: RTOG Protocols: D2cm versus PTV..... | 55 |
| Figure 25: RTOG Protocols: CI versus APR..... | 56 |
| Figure 26: RTOG Protocols: R50% versus APR..... | 56 |
| Figure 27: RTOG Protocols: D2cm versus APR | 57 |
| Figure 28: Change in Dmax (30mm ³) for OAR | 59 |

I. INTRODUCTION

Lung cancer incidence is of growing concern across the world. In the U.S. it has seen an increase in mortality rate among the female population – from 3% of all cancer related deaths in the 1950s to 28% in 2008. Within the male population, its occurrence registered an increase during the 1980s, but has since declined from 1992 onwardsⁱ. Worldwide, lung cancer accounted for 1.37 million deaths in 2008, which was 18% of all cancer related deaths. The occurrence and mortality patterns exhibited by lung cancer closely follow cigarette smoking, with an interval of 20 years. Tobacco consumption in various forms annually account for 71% of all lung cancer related deaths across the worldⁱⁱ.

Because of its high incidence and mortality rates, lung cancer has attracted significant research efforts in terms of conventional drug delivery as well as radiotherapy. Molecular characterization of the disease has led to the development of targeted kinase inhibitor delivery, while the fields of interventional pulmonology and surgical resection of epithelial lung cancer have also witnessed progress. In the field of radiotherapy, the challenges involve tumor motion due to respiration, lung tissue interface heterogeneity, radiation dose to organs at risk, and effective dose delivery. A number of strategies have been delivered in order to meet these challenges, such as 3 Dimensional Conformal Radiation Therapy (3DCRT), Intensity Modulated Radiation Therapy (IMRT), Volumetrically Modulated Arc Therapy (VMAT), Stereotactic Body Radiation Therapy

(SBRT), Positron Emission Tomography (PET) mediated biological targeting, and other treatment methodsⁱⁱⁱ. Procedures for lung cancer surgery (thoracotomy of non-small cell lung cancer) have improved to include removal of single or multiple lobes, removal of a whole lung or a section of it, and removal of lymph nodes. These are sometimes being replaced by non-invasive procedures that deliver a calculated radiation dose to a specific part of the organ at high precision levels.

It is expected that improvements in radiotherapy methods and non-invasive radiosurgery techniques will lead to a better prognosis as well as quality of life for patients suffering from lung cancer.

A. Purpose: Correlating RT and MC Dose Calculations

The purpose of this research is to determine the feasibility of introducing the Monte Carlo (MC) dose calculation algorithm into the clinical practice. The Ray Tracing (RT) algorithm significantly overestimates the dose delivered as compared to the MC algorithm for lung^{iv}. Unlike the RT, the MC algorithm is not affected by the tissue inhomogeneities, which are significant inside the chest cavity. This study will quantify this overestimation and identify significant correlations between the RT and MC calculated dose distributions. Additionally, the data will be subdivided into size and density regimes to attempt to maximize the correlation between the PTV volume and the dose coverage changes. The changes in RTOG 0813 protocol criteria and Organs at Risk (OAR) will also be recorded and analyzed.

B. Lung Cancer

Lung cancer incidence has been associated primarily with tobacco intake, but the International Agency for Research on Cancer (IARC) has also identified arsenic, asbestos, cadmium, and other industrial pollutants as contributing carcinogenic agents. The industries that have been identified as high risk for this disease are asbestos mining, textile manufacturing, construction, insulation, and those that involve significant long-term exposure of workers to diesel fumes^v. Another common agent that has been identified is radon gas, which can be found in households as well as in deep mineshafts. Apart from these environmental factors, a degree of genetic predisposition towards lung cancer has also been observed. For example Samet, Humble, and Pathak^{vi} showed that the risk of lung cancer for an offspring increased five times if at least one of his or her parents was diagnosed with lung cancer. This study also concluded that those with a family incidence of lung cancer were at increased risk if they also used tobacco.

Lung carcinogenesis is divided into two types – small cell carcinoma (SCLC) and non-small cell carcinoma (NSCLC). NSCLC is in turn of three types – adenocarcinoma, squamous cell lung carcinoma, and large cell lung carcinoma. NSCLC represents 80-85% of the incidence of lung cancer, while the balance is accounted for by SCLC. Both these types have been observed to occur through anomalous signaling that result in growth-stimulant pathways switching on and oncogene activation through mutation, overexpression, and other pathways. Lung cancers have also been associated with anomalous behavior of the Receptor Tyrosine Kinases (RTKs), usually resulting in the occurrence of anomalous fusion proteins. Some of the common oncogenes that have been identified are MET and Epidermal Growth Factor Receptor (EGFR), while the

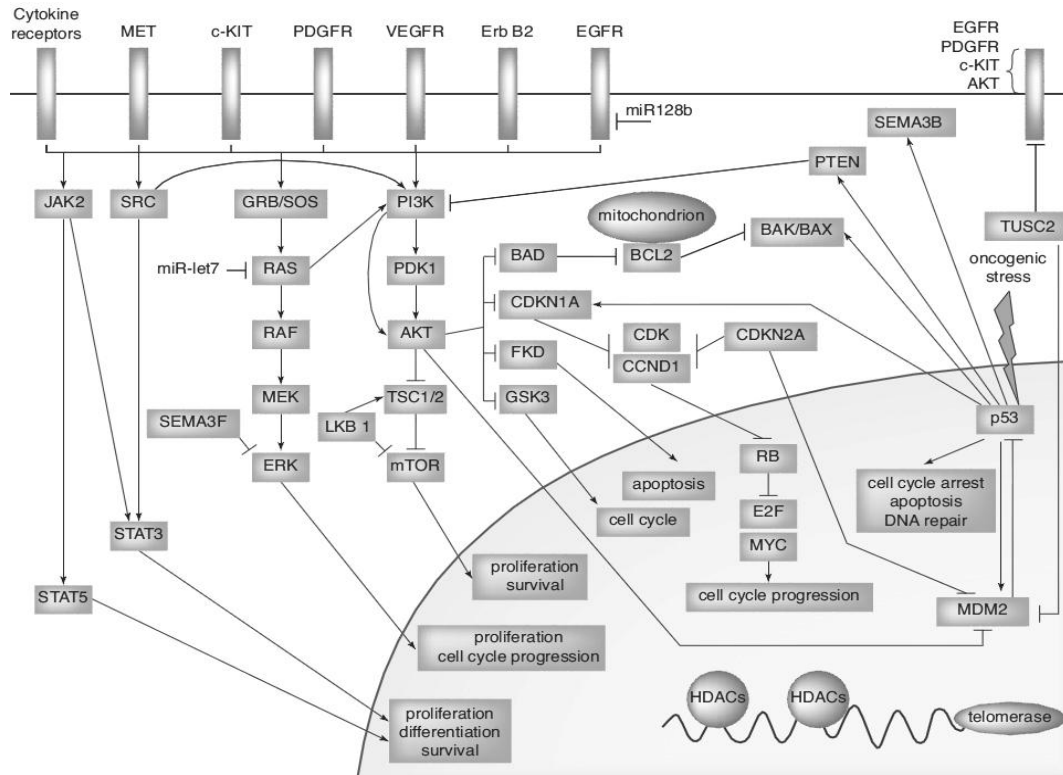


Figure 1: A study of signaling pathways involved in lung cancer^{vii}.

inactivation of TSGs has also been associated with the onset of carcinoma^{vii}. Figure 1 shows a detailed study of the signaling pathways responsible for both types of lung cancer.

Diagnosis of lung cancer is performed by tissue recovery, usually through percutaneous lung/lymph node biopsy or through a variety of bronchoscopy techniques. Post diagnosis, the course of therapy is determined by staging. Staging can be either clinical or pathological. The former involves clinical examination and radiography, CT, PET, MRI, or other imaging methods. The latter involves a histology tissue examination, with the tissue obtained through Endo Bronchial Ultra Sound (EBUS), Endoscopic Ultra Sound (EUS) or other methods. The Tumor-Node-Metastases (TNM) process is used for

classification, as recommended by the International Association for the Study of Lung Cancer (IASLC)^{viii}.

Post staging, the treatment method is applied: surgery, radiotherapy, chemotherapy, or an appropriate combination. Most lung cancers, especially in the early stage (I and II), and those involving NSCLC are treated by a surgical procedure. If a patient is deemed to be at risk from surgery, then radiotherapy is recommended. Various dose delivery techniques are available and will be discussed later in this report. Those in an advanced stage (III and IV) are offered chemotherapy, either as a stand-alone procedure or in conjunction with neoadjuvant radiotherapy and surgery. Advanced stages of metastasis are treated solely with chemotherapy.

One of the chief causes of mortality in any form of cancer is metastasis. In case of lung cancer, the metastatic pathway is either through the lymphatic or through the vascular network, as shown in Figure 2. Out of these, the former represents the dominant pathway because of the utilization of thoracic ducts by the cancerous cells. Metastasis through the lymphatic pathway, or lymphangiogenesis, is mediated by the growth factors VEGF-C and VEGF-D. The other pathway, representing hematogenous carcinoma, has very poor prognosis. Tumor cell spread via this mechanism is mediated by growth factors VEGF-A, VEGF-C, and VEGF-D^{ix}.

C. Radiation Therapies

As already stated, radiation therapy is recommended procedure for patients diagnosed with an early stage of lung cancer and those who are at risk from surgery. Within the thoracic cavity, the organs at risk (OAR) from radiation are the lungs,

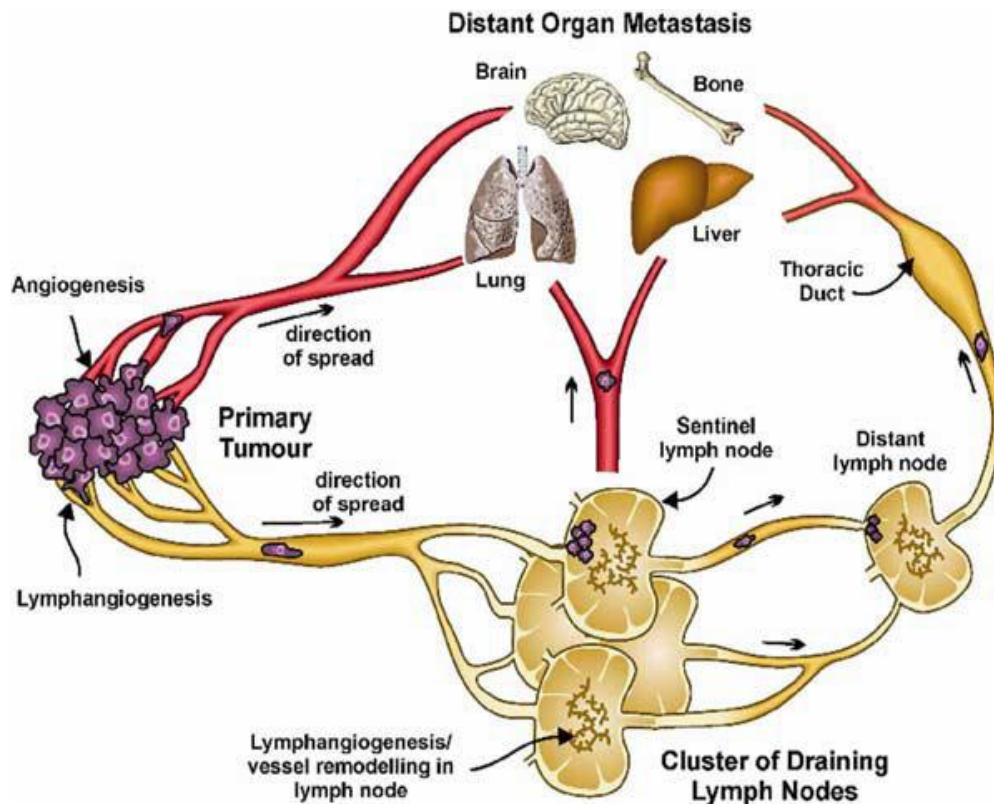


Figure 2: Schematic diagram of lung cancer metastases. Red represents blood vessels and yellow represents the lymphatic network^{ix}.

esophagus, ribs, heart, great vessels, trachea and main bronchi, and the spinal cord. The effect on these OARs must be carefully evaluated before radiotherapy and various groups (such as the Radiation Therapy Oncology Group, RTOG; European Organization for Research and Treatment of Cancer; and Southwest Oncology Group, SWOG) have determined the upper limits of dose delivery for these organs^x. Table 1 lists the upper dose limits for OARs in the thoracic cavity.

Table I: Dose limits for OARs in the thorax. V_{20} denotes the percentage of lungs that receives dose greater than 20Gy, fx denotes fraction^x.

| Dose limits for OARs | 3D-CRT (RTOG 0617) | 3D-CRT (RTOG 0972/CALGB 36050) | SBRT (RTOG 0618, 3 fx) | SBRT (ROSEL European trial, 3 or 5 fx) |
|------------------------------|---|---|-------------------------|--|
| Spinal cord (point dose) | Point dose ≤ 50.5 Gy | Any portion ≤ 50 Gy | ≤ 18 Gy (6 Gy/fx) | 18 Gy (3 fx) |
| | | | | 25 Gy (5fx) |
| Lung | Mean lung dose ≤ 20 Gy, $V_{20} \leq 37\%$ | $V_{20} \leq 35\%$ | $V_{20} \leq 10\%$ | $V_{20} < 5-10\%$ |
| Esophagus | Mean dose ≤ 34 Gy | Not limited | ≤ 27 Gy (9 Gy/fx) | 24 Gy (3 fx) |
| | | | | 27 Gy (5 fx) |
| Brachial plexus (point dose) | ≤ 66 Gy | Not limited | ≤ 24 Gy (8 Gy/fx) | 24 Gy (3 fx) |
| | | | | 27 Gy (5 fx) |
| Heart | $\leq 60, \leq 45, \leq 40$ Gy for 1/3, 2/3, 3/3 of heart | $\leq 60, \leq 45, \leq 40$ Gy for 1/3, 2/3, 3/3 of heart | ≤ 30 Gy (10 Gy/fx) | 24 Gy (3 fx) |
| | | | | 27 Gy (5 fx) |
| Trachea, bronchus | Not limited | Not limited | ≤ 30 Gy (10 Gy/fx) | 30 Gy (3 fx) |
| | | | | 32 Gy (5 fx) |
| Ribs | Not limited | Not limited | Not limited | Not limited |
| Skin | Not limited | Not limited | ≤ 24 Gy (8 Gy/fx) | Not limited |

Radiation oncology works primarily by damaging the DNA strands of cancerous cells. Depending on the positioning of the radiation source, it can be divided into three types: External Beam Radiotherapy (EBRT), sealed source radiotherapy or Brachytherapy, and unsealed source radiotherapy (the last utilizes a soluble radioactive salt to achieve targeted destruction of carcinogenic cells). Brachytherapy and EBRT are discussed in this report.

1. Brachytherapy

Brachytherapy is a type of conformal therapy, and can be defined as delivery of irradiating beams at close range to the target cells. This allows delivery of hyperdose to the cancer cells, sufficient dose to the tissue interface, and minimal dose to normal tissues surrounding the tumor^{xi}. The method involves introduction of radiation sources (known as seeds) in near vicinity of the tumor source. Commonly used seeds are Iridium-192 (^{192}Ir), Iodine-125 (^{125}I), and Palladium-103 (^{103}Pd). Earlier the presence of inhomogeneity such as bone was ignored, and the American Association of Physicists in Medicine (AAPM) Task Group 43 (TG-43) recommended dose planning based on homogenous medium. Later, however, work was done to account for inhomogeneity – for example by Slate et al.^{xii}, who used a Monte Carlo simulation to study the effectiveness of dose prediction in the presence of bone.

The International Commission on Radiation Units and Measurements (ICRU) defined three types of brachytherapy depending on the dose limits used: Low Dose Rate (LDR) with a rate of 0.4-2 Gy/hr (sometimes extended up to 1.9 Gy/hr), Medium Dose Rate (MDR) with a rate of 2-12 Gy/hr, and High Dose Rate (HDR) with a dose rate above 12 Gy/hr^{xiii}. Pulsed Dose Rate (PDR) brachytherapy, in contrast, uses a high number of smaller doses in order to combine the advantages of LDR and HDR. Another way in which brachytherapy is classified is based on radioactive source location: intracavity (source is placed within the body cavity in near vicinity to tumor), interstitial (source is surgically implanted within the tumor volume), surface or mold (source placed over the tumor), and intraluminal (source located inside a lumen). In case of interstitial placement, the source can be placed either in an intraoperative or in an intravascular

manner. The implant can also be either temporary (removed after a prescribed dose has been delivered) or permanent (source is allowed to deliver its complete dose and decays within the body). Intra-cavity and interstitial brachytherapy are used most frequently^{xiv}. A recent development in brachytherapy has been image guidance, in which a target volume enveloping the implant can be defined and dose delivery can be calculated (similar to external beam radiotherapy).

In order to reduce the danger of radiation exposure of physicians and staff, the technique of afterloading has been developed. This is performed in two stages – emplacement of a non-radioactive applicator in the cancer patient followed by placement of the radioactive source. In manual afterloading, typically used for LDR treatment, the source is placed manually by a staff wearing shielding equipment. This has a high probability of exposing the operator or staff to radiation. On the other hand, remote afterloading allows the use of a microprocessor guided machine in a shielded treatment room for placing the source within the carrier. This has very little chance of exposing staff to radiation, and is followed in HDR as well as LDR treatment procedures^{xv}.

Dose calculation in brachytherapy has traditionally followed the “Manchester system”, which recommends arranging the radiation sources according to precise geometrical configurations. Dose delivery of isotope of different elements is calculated in milligram equivalents by converting these into radium substitutes. The equivalence is calculated by taking into account the same dose rate at the same distance from the source, and is expressed by the equation,

$$Ra_{eq} = A \frac{\Gamma}{\Gamma_{Ra}},$$

where A represents the source activity, Γ is its exposure rate constant and Γ_{Ra} is the exposure rate constant of radium. The value of radium equivalence is determined experimentally in air equivalent ionization chambers^{xvi}. The Biological Effective Dose (BED) is calculated as a fraction of the total dose D by multiplying it with a factor:

$$BED = D \left(1 + \frac{d}{(\alpha/\beta)} \right),$$

where the total dose D is delivered in n fractions of dose d each. If the dose rate is denoted by R and treatment time by T, then $D = RT$ and the above equation can be expressed for LDR therapy as

$$BED = RT \left(1 + \frac{2R}{\mu(\alpha/\beta)} \right),$$

where μ is the sub-lethal damage (SLD) repair rate constant^{xi}. Interstitial brachytherapy is often used for lung cancer in early stages as well as for lesions within the bronchus. The advantage of brachytherapy is that it allows dose delivery to a localized target volume and constant irradiation of the tumor; its disadvantage is that it cannot be used for non-localized or larger tumors and it may lead to bleeding, tissue swelling, and other discomforts to the patient^{xvii}. Brachytherapy has traditionally been most effective in treating gynecological and prostate cancers.

2. External Beam Radiation Therapy for Lung Cancer

In contrast to brachytherapy, external beam radiotherapy employs high energy X-ray beams to destroy carcinogenic cells. An earlier method involved delivering a 2 dimensional beam to the treatment volume without control over dose delivered to healthy tissue; this has now been largely supplanted by 3 dimensional conformal therapy using

multi-leaf collimators and other techniques. Some of these therapies are discussed in the next sections.

a. 3D Conformal Radiation Therapy (3DCRT)

Any conformal radiotherapy procedure aims to irradiate an irregularly shaped target with a homogenous dose while at the same time avoiding normal tissue adjacent to the treatment volume. 3D radiotherapy as a conformal planning and delivery system of ionizing radiation has been in development since the 1980s. It has led to better dose control in the treatment of cancer of a number of areas, including head and neck, lung, breast, and prostate. 3DCRT has been made possible mainly due to advances in two areas – imaging techniques and dose delivery technology. Variations in beam geometry are achieved through use of wedge or compensator blocks, or through multi leaf collimator restricted fields. In order to calculate dose distribution, different algorithms are used – these can be either measurement-based or model-based. The former utilize water or tissue equivalent phantoms to calculate the dose distribution in patients, while the latter employ computer generated models for the same calculations. While the former method is more accurate since it can take tissue inhomogeneity effects into consideration, the latter is usually faster^{xviii}. An example of 3DCRT is shown in Figure 3, where the planning target volume (PTV) is shown in red. Several opposed beams are used to create a high isodose region within the PTV.

Surrounding normal tissue are contoured in the tomography image and shown as 3D surfaces. Beams are delivered using different gantry and couch positions such that normal tissue is not irradiated by all the beams simultaneously. A comparison between

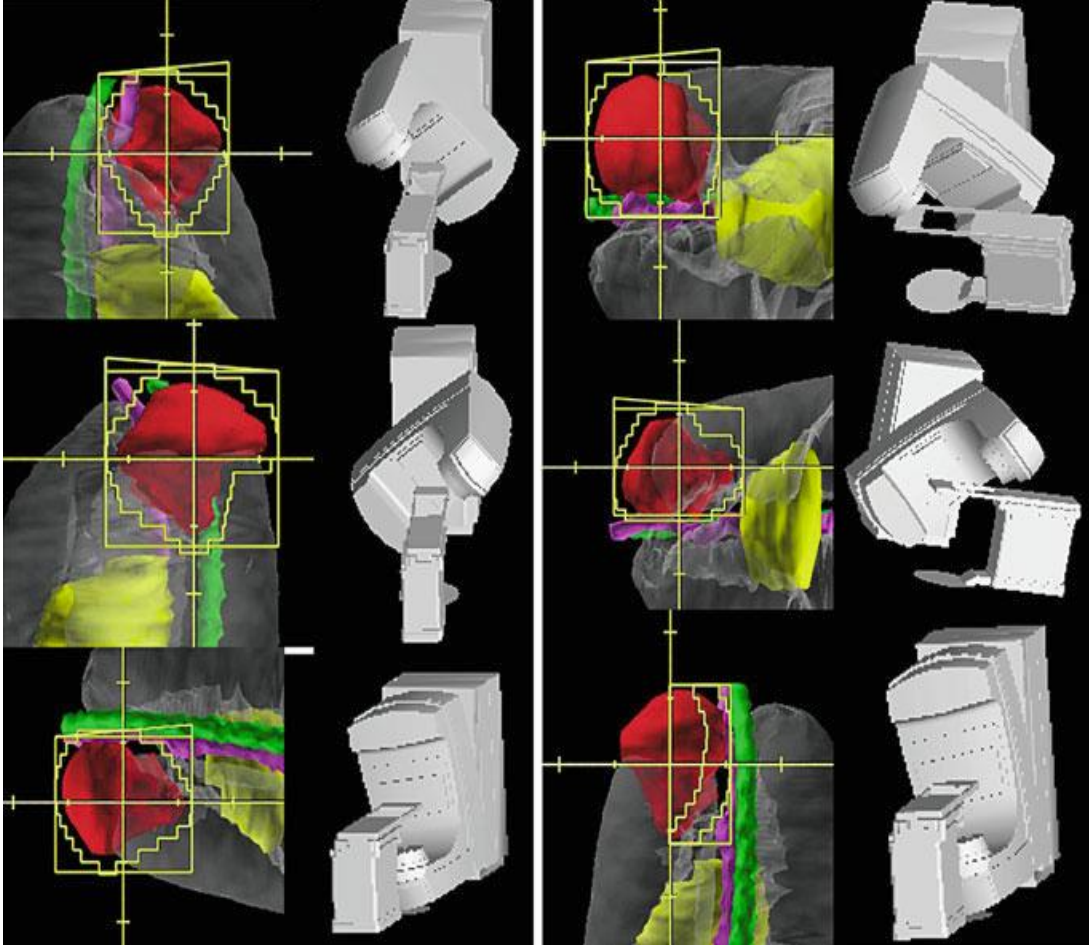


Figure 3: 3DCRT of a tumor (denoted by red) in the left upper lobe^{xix}.

3DCRT and IMRT plan generation in a complex target geometry showed that IMRT was more effective in avoiding dose delivery to healthy tissue. 3DCRT had a better target coverage, but also delivered excessive planned dose to the spinal cord^{xx}.

b. IMRT-IGRT

While 3DCRT achieves spatial localization of the radiation beam, it still cannot yield an accurate treatment plan for tumors that have highly convoluted shapes or when critical organs are in the vicinity. Intensity Modulated Radiation Therapy (IMRT) goes a

step further in this direction by modulating the intensity of radiation beam during each dose delivery.

IMRT uses computerized beam control and intensity variation to conform to the target shape in three dimensions. In an ideal situation, the radiation beam should be conformed to the shape of the tumor at each beam angle for optimal delivery of radiation dosage. IMRT aims to achieve this by use of Multi Leaf Collimators (MLCs) that are controlled by a computer to create several openings at each desired angle, thus modulating the radiation. The radiation is segmented into various shapes by the leaves by varying them into different positions from “open” to “close”, and this gives high conformity with complex tumor shapes. Figure 4 shows a comparison between traditional radiotherapy and computerized IMRT. For conducting an IMRT session, at first an anatomical and structural plan is prepared by contouring and identifying dosage constraints, together with their weightings. The incident beam is then divided into numerous small beam-lets, varying in intensity from 0% to 100%, through software that uses several iterations to prepare the optimal dosage plan. Any IMRT procedure takes into account several factors, such as dose distribution, extent of coverage of the target, delivery time, time needed from the planning stage to actual delivery, quality assurance etc. IMRT uses various delivery techniques such as Modulated Arc Therapy, Dynamic Arc Therapy, Step-and-Shoot Delivery and combinations of the above. IMRT treatments can be administered with the MLCs operating in any one of three basic modes: Segmented MLC (SMLC) mode, or the step-and-shoot mode, Dynamic MLC (DMLC) mode, or the sliding window mode, and Intensity Modulated Arc Therapy (IMAT). In the step-and-shoot mode the IM fields are divided into a sequence of small sections or sub-

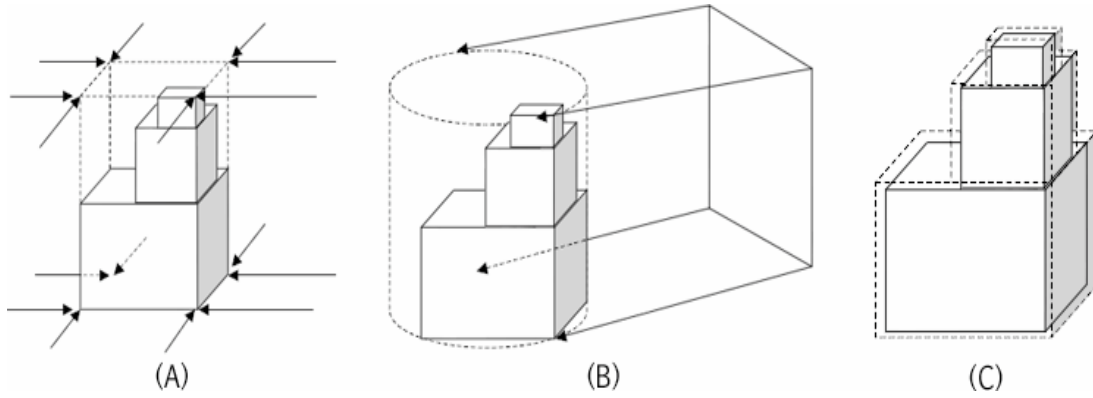


Figure 4: Comparison between IMRT and conventional radiotherapy. (A) non-conformal therapy without blocking (B) rotational therapy where the uniform-intensity beam is rotated through an angle of 2π (C) intensity-controlled field that is also geometrically shaped by using MLCs – the goal of IMRT^{xxi}.

fields, each having a uniform intensity value. The beam is switched on only when the leaves are in a stationary position in each of the prescribed sub-field positions, and the MLC does not move while the beam is on. Step-and-shoot IMRT can be performed with “forward” and “inverse” planning. In the former, the oncologist uses a number of placements of the MLCs manually to deliver a homogenous dose distribution. The final dosage is calculated from a Dose Volume Histogram (DVH) of the target tissue and the surrounding tissue that is to remain unaffected. On the other hand, in “inverse planning” the physician develops the desired DVH, while the treatment planner sets the dose objectives and constraints. An algorithm uses several iterations to calculate an optimum fluence pattern that is best suited to meet the objective. While Pencil Beam (PB) convolution/supervision algorithms are most common for IMRT, application of Monte Carlo based simulation algorithms has also been investigated^{xxii, xxiii}.

Usually less than 10 Monitor Units (MUs) are used with several segments, thus necessitating a performance of the accelerator within required safety levels at a minimal interval from its startup. During the initial starting period, the beam energy can have a slightly different value from its designated value, depending on the design employed, and this can affect different beam characteristics such as dose/MU, Percentage Depth Dose (PDD), and the profile of the beam. Hence it is essential to calculate the startup characteristics of the accelerator during its pre-deployment trial, as well as check the characteristics on a regular basis as part of QA^{xxiv}.

In the DMLC mode the IM fields are delivered dynamically with the leaves of the MLC moving into different positions during irradiation. A computer controls the movement so that each pair of opposite leaves creates an opening; this opening moves across the intended delivery volume. The radiation is kept on during the whole process in order to achieve the fluence map determined earlier. The accumulated intensity of radiation at each point is proportional to the interval during which one leaf opens over the point and the next leaf closes over it. Delivering the determined intensity profile requires the appropriate correlation between the speeds of each leaf pair, not a correlation in time. An important check of the DMLC mode is whether the leaf system moves at the same uniform speed that the calculation algorithm uses to calculate the leaf motion.

A variety of Image Guided Radiotherapy (IGRT) techniques have also been developed along with IMRT. For example, Single Photon Emission Computed Tomography (SPECT) is a method of acquiring tomographic images of the body using gamma rays emitted by a radioisotope (usually Technetium 99). It utilizes single or multiple rotating gamma cameras to acquire a series of 2D images, projections, of the

human body from different angles. A radioisotope attached to a binding ligand is administered to the patient prior to the imaging process, and the concentration of the ligand in the organ of interest is then imaged by the gamma camera. The data obtained from the camera is then processed to remove noise and other types of errors, and reconstructed into images using a variety of algorithms. SPECT imaging is used for a multitude of diagnostic purposes, including cardiac study, brain imaging, investigation of tumors etc. Commercial SPECT systems use single or dual rotating gamma cameras in order to capture data, from which tomographic images are constructed. The images are constructed at resolutions of 64 x 64 or 128 x 128 pixels. A series of contiguous images, or slices, of the volume under investigation are pieced together to build-up a 3-D image of the volume. SPECT has been found to be particularly useful for tumor detection and localization in the thorax, abdomen, and brain^{xxv}. Parallel-hole collimators usually need 64-128 views at a distance of 20-60cm; for higher resolution and data correction requirements, a full 360° Field-of-View is usually captured. Since computer screen sizes are normally 1024 x 768 with 16 bit or higher color depth, linear interpolation is used to approximate the additional pixels^{xxvi}. SPECT imaging is replaced by Positron Emission Tomography (PET) when images with higher sensitivity are required, since PET cameras can record a greater number of emission events than SPECT cameras^{xxvii}.

c. RapidArc IGRT

RapidArc is a radiotherapy technique developed by Varian Medical Systems. It employs Volumetric Modulated Arc Therapy (VMAT) along with single or double arc

gantry rotations. In order to develop a conformal dose delivery regime, it employs MLCs as well as variations in dose rate and gantry positions. The dose rate is varied continuously through MLC leaf motion as the linac traces an arc. While IMAT is somewhat similar to dynamic VMRT in that both therapies use MLC movement during beam-on, the former allows a more sophisticated treatment planning and delivery program. For a given treatment plan quality, RapidArc can perform its therapy more quickly delivering less number of Monitor Units (MUs) than a DMLC system^{xxviii}. Since VMAT plans can take advantage of more advanced MLC configurations such as positioning leaves in the beam path and small MLC openings, there is also a correspondingly greater need for performing commissioning and quality assurance (QA) for equipment such as RapidArc.

Van Esch et al.^{xxix} performed a comprehensive study of machine and patient QA as well as treatment planning system (TPS) for such a system under a variety of conditions. The measurement devices used were Gafchromic film, a standard ion chamber array, and an Electronic Portal Imaging Device (EPID). For the TPS validation program, the authors observed good agreement with calculated dose at different collimator positions (within 2%), while greater resolution in fluence calculation was achieved. In another comparison between VMRT and RapidArc, Seppala et al.^{xxx} studied possible calculation errors and dose build-up for small lung tumor irradiation. Lung heterogeneity was simulated using two polycarbonate phantoms, and dose distribution was calculated using pencil beam convolution (PBC) and anisotropic analytic algorithm (AAA). They observed that the high definition MLCs (HD-MLCs), employed in the equipment, were able to generate very small field sizes, but this also affected the

peripheral dose distribution. In fact the highest difference between the observed and calculated isodose lines occurred at a sliding window aperture size of 2mm, and at this size the PBC failed to predict the peripheral dose accurately. From this study, it is evident that the RapidArc should be operated with an aperture size of 6mm or higher. It seems, however, that AAA performs slightly better for smaller aperture sizes; while it still calculates lower doses and higher spread, the results can be improved by using a smaller calculation grid. This is especially true for increased MUs, in which a 1mm grid resolution should be used even though it increases the calculation time^{xxxix}.

d. Cyberknife

The CyberKnife is a stereotactic IGRT system developed by AccuRay, Inc. It deploys an X-band 6MV linac on a robotic arm in order to provide sub-millimeter accuracy during patient treatment^{xxxix}. The arm has multiple joints and has 6 degrees of freedom, enabling it to achieve a series of positions (called nodes) during treatment. At each node the CyberKnife TPS obtains two images, calculates the patient position, cone size, and MUs and makes necessary corrections^{xxxix}. Figure 5 shows the volume covered by the robotic arm of CyberKnife:

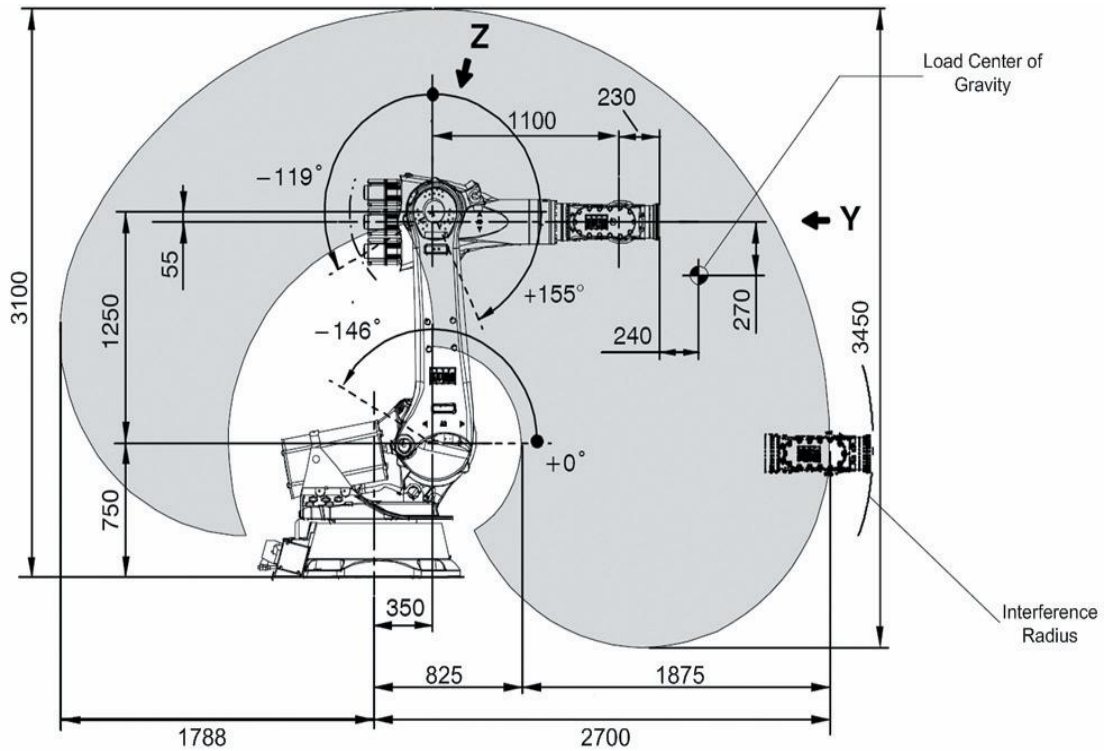


Figure 5: Side view of the axes of movement and volume covered by CyberKnife's robotic arm^{xxxiv}.

For tracking tumors in real-time, the system uses the Synchrony Respiratory Tracking System, which continually compares X-Ray images of the tumor with an external breathing signal that is updated in real-time. The breathing signal and the tumor motion are correlated by a software model, which positions the arm at the beginning of each node. However, there is a lag of 115 ms for each beam positioning and a predictive algorithm is used to compensate for the lag. In actual practice, a combined algorithm that takes data from three separate prediction algorithms has been observed to yield an accuracy of less than 1mm. Another type of error that the Synchrony system compensates for is the relative motion between the internal tumor and external chest or abdomen movement. Another module, the Xsight Lung Tracking system, can perform respiratory

tracking and does not require emplacement of fiducial markers for spine treatments^{xxxv}.

A clinical study of the Synchrony system, during treatment of 70 patients having Stage I NSCLC, was performed by Zyp et al.^{xxxvi} 59 patients received a dose of 60 Gy and 11 patients received a dose of 45 Gy, both groups receiving the dose in 3 fractions. The authors reported a very high local control of 96% at 1 and 2 years for the former group, while the second group had a 78% actuarial control rate. 10% of all the treated patients exhibited grade 3 toxicity related to the treatment. All patients were allowed to breathe normally, and even those having inferior lung function underwent therapy by virtue of different marker placement methods. This shows that the CyberKnife can be a viable treatment system for lung cancer patients.

i. Stereotactic Body Radiation Therapy (SBRT)

The CyberKnife is a Stereotactic Body Radiation Therapy (SBRT) unit, employing a co-ordinate system to treat localized tumors with accurate radiation dosage. The co-ordinate system allows delivery of a higher BED to a relatively smaller area with sharp drop-off, thus lowering associated toxicity levels. SBRT brings together advances in imaging, dose simulation, TPS, and dose delivery. While conventional 3DCRT and IMRT deliver 1.8-3 Gy in 10-30 fractions, SBRT delivers as much as 6-30 Gy in 1-5 fractions. However, the application of SBRT requires tumors with well-defined boundaries, so that gross tumor volume (GTV) equates exactly to the clinical target volume (CTV). In addition, the radiobiological principles behind SBRT are less understood than in the case of IMRT^{xxxvii}. Because of the requirement of precise tumor demarcation, SBRT requires acquisition of 3D data sets from a four dimensional

computed tomography (4DCT) system for dose calculation. Image acquisition through MRI and PET scans is also used for SBRT visualization. While planning a SBRT session, the lung is divided into two regions – central and peripheral. This is shown in Figure 6, in which a thick green line denotes the proximal bronchus tree and a dashed green line denotes the division between the central and peripheral lung. A constant 2-cm expansion in all directions, except in the superior, from the proximal bronchus tree is shown^x.

Treatment planning in SBRT involves identifying a small volume that contains the gross tumor and its immediate periphery. Since high doses are delivered in each fraction, local hotspots develop within the target volume, but this is deemed acceptable. Development of IGRT techniques now mean that patients need to be scanned in a body frame with fiducial implants; even rotational effects in three dimensions can be compensated to some effects by using robotic couches^{xxxviii}. In case of lung SBRT, clinical changes that have been observed are sub segmental or wedge shaped fibrotic tissue development that continue distally. This is most probably due to the serial-parallel tissue structure of the lungs^{xxxix}.

An RTOG 0236 study conducted by Timmerman et al.^{xi} involving 59 patients with early stage lung cancer showed good results when treated with SBRT. They exhibited a survival rate of 55.8% and primary tumor control rate of 97.6% at 3 years; they also had moderate treatment induced morbidity. The group concluded that SBRT can result in twice the primary tumor control rate observed in other types of radiotherapy. The trial followed the protocols published by the RTOG and ACR^{xli}. Results are expected from the RTOG 0813 and 0915 studies.

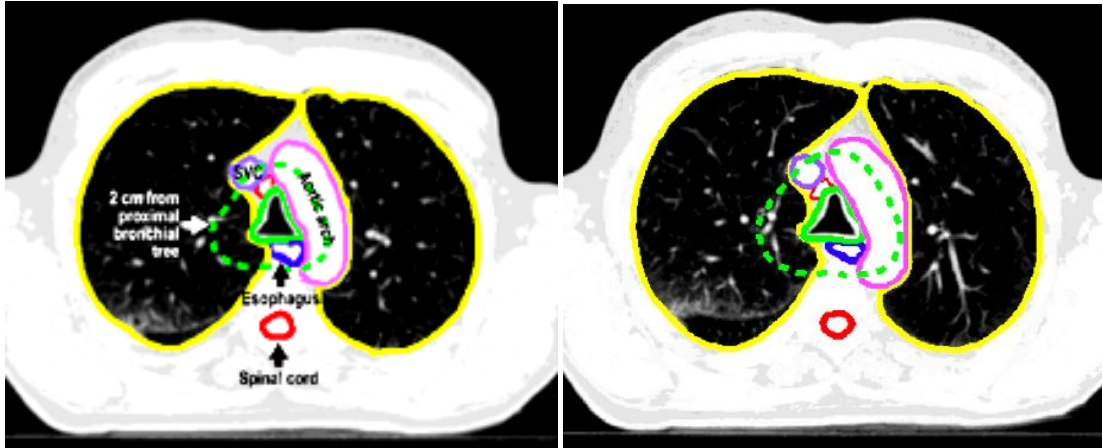


Figure 6: Color coded lung atlas showing different regions. Red line denotes spinal cord, yellow line denotes the lung, dark blue denotes esophagus, light blue denotes superior vena cava, purple denotes aortic arch and thin red denotes a tumor^x.

ii. RTOGs/ SBRT For Lung Cancer

The Radiation Therapy Oncology Group has published protocols for conducting SBRT trials in its reports RTOG 0236, 0618, 0813, 0915, and 0631. RTOG 0618 states that 75% of bronchogenic carcinoma cases present with NSCLC, and out of the latter 15-20% cases present with Stage I NSCLC (Stage I cases are expected to rise because of early diagnosis made possible by CT imaging). While surgical resection is the preferred treatment method for such cases, with high 5-year survival rates, the report states that those who are at risk from surgery may undergo radiotherapy, with a 5-year survival rate between 10-30%. Such patients undergoing conventional radiotherapy are administered a total of 45-66 Gy with 1.8-2.0 Gy in each fraction. However, the local dose rate can be increased significantly in 3DCRT and SBRT; in case of the latter, studies have shown the administration of 20-22 Gy in each of 3 fractions (a total of 60-66 Gy). Dose limiting

toxicity (DLT) in each of the studies was taken as grade 3 pulmonary, but prohibitive toxicity levels were not observed in most of the patients undergoing SBRT (pneumonitis and hypoxia were observed for individual patients in an Indiana University study)^{xlii}. RTOG 0813 discusses aspects of primary tumor control and toxicity, and comments that several aspects of SBRT differ between institutes. This report proposed an alternative to earlier Phase I studies, replacing a standard progression of patients from Phase I to Phase II by the method of continuous reassessment methodology (CRM). CRM is a statistical technique in which any DLT observed in one patient determines the dose delivered to the next patient, thus ensuring that all patients taking part in the study contribute towards developing the maximum tolerated dose (MTD). In a further refinement, patients are accrued on a continuous basis if adverse reactions are observed after a delay – this is known as the Time-to-Event Continual Reassessment (TITE-CRM) technique^{xliii}. RTOG 0631 discusses the suitability of IGRT/SBRT for spinal oligometastases. Based on earlier studies, the delivered dose through conventional radiotherapy is limited to 10 Gy to 10% of the spinal cord, which is the OAR for the study. In case of IGRT/SBRT, the proposed dose delivery is 16 Gy or 18 Gy in a single fraction. The object of the study is pain control, as evaluated by the Numerical Rating Pain Scale (NRPS), 3 months after the therapy session^{xliv}.

D. Treatment Planning for Cyberknife

The CyberKnife treatment planning system, commercially known as the MultiPlan System, conventionally employs the Ray Tracing algorithm for dose calculation, with adjustments of some parameters for patient geometry. The parameters

are: off-center ratios (OCR), tissue-phantom ratios (TPR), and collimator output factors (OF). These are calculated under standard conditions and an additional coefficient, the central axis effective depth calculation (d_{eff}), is used to correct for tissue heterogeneity. In case of low density heterogeneity additional electron transport and scatter inequalities may develop, but these are not compensated^{xlv}. Because of the relatively simple algorithm employed, the treatment planning may lead to significant differences in planned and delivered doses, thus leading to a higher toxicity level as well as lower tumor control^{xlvi}. The dose delivered per MU (cGy/MU) is estimated by the following equation:

$$D/MU = OCR(coll, R_{800}, d_{eff}) \times \left(\frac{800}{SAD} \right)^2 \times TPR(FS, d_{eff}) \times OF(coll, SAD).$$

Since lung tissues present more heterogeneities than the brain, it can be observed that the above equation may not be adequate for calculating dosage values for the small field sizes that the CyberKnife employs. In order to overcome this, the MultiPlan Treatment Planning System v2.1 and above offers an optional Monte Carlo module, which is available for both fixed and variable aperture collimators^{xxxiv}. The Monte Carlo algorithm employed uses several variance reduction routines in order to increase calculation efficiency, including: photon interaction forcing, particle splitting, Russian roulette, track repeating etc. Three voxel resolutions are supported: low (128 x 128), medium (256 x 256), and high (512 x 512). The number of photons that are used in the calculation is obtained from two parameters: uncertainty of the result, selected by the operator and the number of voxels in the CT volume covered by the patient model. The dose calculation is performed in a loop that also accounts for tissue type and density, and the loop is repeated as long as there are photon interactions remaining within the tracked volume.

Calculations time depends on the level of uncertainty chosen and can be improved by using multithreading or multi-core processors^{xlvi}. Typical calculation times for lung, head and liver regions at both high and low resolutions were estimated by Ma, Li, Deng, and Fan^{xxxiii}; for the lung area it varies between 0.68-5.4 minutes using a multithreaded processor. Table II below shows the different simulation times obtained at a 2% uncertainty level. MCRS denotes the algorithm actually employed, MCSIM denotes a benchmarked algorithm previously developed by Ma et al.^{xlvi} Both these employ variance reduction techniques mentioned before, while full MC does not employ the techniques. Figures in brackets denote the ratios by which MCSIM and MCRS were faster than full MC. The two algorithms employed for dose calculation in the CyberKnife, Ray-Tracing and Monte Carlo, are discussed in more detail in the next two sections.

Table II: Calculation times using different options of the MC algorithm in CyberKnife^{xxxiii}.

| Organ | Voxel size (mm) | Target size (cc) | No of voxels | Cone size (mm) | No of beams | Full MC CPU T (min) | MCSIM CPU T (min) | MCRS CPU T (min) |
|-------|-----------------|------------------|--------------|----------------|-------------|---------------------|-------------------|------------------|
| Lung | 3.9 x 3.9 x 3 | 4.03 | 88 | 12.5 | 158 | 57 | 3.5 (16.3) | 1.6 (35.6) |
| Lung | 1.95 x 1.95 x 3 | 4.72 | 413 | 12.5 | 158 | 228.9 | 17.8 (12.9) | 5.7 (40.2) |
| Lung | 3.9 x 3.9 x 3 | 91.6 | 2002 | 20 | 126 | 324.4 | 19.9 (16.3) | 5.9 (55.0) |
| Lung | 1.95 x 1.95 x 3 | 96.5 | 8436 | 20 | 126 | 842.4 | 79.2 (10.6) | 18.8 (44.8) |
| Lung | 3.9 x 3.9 x 3 | 62.1 | 1356 | 25 | 134 | 231.5 | 15.7 (14.7) | 4.5 (51.4) |
| Lung | 1.95 x 1.95 x 3 | 68.4 | 5977 | 25 | 134 | 710.6 | 43.7 (16.3) | 13.4 (53.0) |
| Head | 2.2 x 2.2 x 2 | 0.73 | 74 | 5 | 123 | 35.2 | 2.5 (14.1) | 0.84 (41.9) |
| Head | 1.1 x 1.1 x 2 | 0.86 | 351 | 5 | 123 | 112.9 | 8.0 (14.1) | 2.6 (43.4) |

| | | | | | | | | |
|-------|---------------------|-------|------------|----|-----|-------|-----------------|-----------------|
| Liver | 3.9 x 3.9 x 1.25 | 817 | 42860 | 60 | 232 | 2379 | 171.2(13. 9) | 80.1 (29.7) |
| Liver | 1.95x1.95x1. 25 | 839.7 | 17632 4 | 60 | 232 | 12911 | 807.8(16. 0) | 207.8 (62.1) |

1. Ray-Tracing Algorithm

RT algorithms were probably first used in calculating two dimensional collimator detector response functions (CDRFs) of imaging devices^{xlix}. One of the most important aspects of dose calculation in the patient body is correction for tissue inhomogeneity. RT achieves this by calculating variations in fluence (which is a function of tissue density encountered by the primary beam) at different areas within the patient body. Different correction algorithms have been developed to address this variation, based on how the scattered photons and primary electron are modeled. Out of these one of the oldest commercially implemented correction methods was the Ratio of Tissue-Air Ratios (RTAR), which used the concept of radiological depth in order to approximate a series of TAR values. A better inhomogeneity correction factor (ICF) was the Batho Power Law and its derivative, the modified Power Law. The former is given by the equation

$$ICF = \frac{TAR(d_1, W_d)^{\rho_1 - \rho_2}}{TAR(d_2, W_d)^{1 - \rho_2}},$$

where ρ_1 and ρ_2 are the relative densities of the calculation medium and overlying medium respectively, d_1 and d_2 are depths of the calculation medium and initial point of the overlying medium respectively, and W is the field size^l. This was modified by Webb, Fox, Cassel, and others to provide the following equation:

$$ICF = \prod_{m=1}^{m=N} TAR(X_m)^{(\rho_m - \rho_{m-1})/\rho_0} \frac{(\mu_{en}/\rho)_N}{(\mu_{en}/\rho)_W},$$

where N represents the number of distinct layers, m is the number assigned to a particular layer, x_m is the distance to the initial point of the m th layer, ρ_μ and ρ_0 are densities of the m th layer and of water respectively, and $(\mu_{en}/\rho)_N$ is the absorption coefficient for layer N^{xlix} . The above are examples of 1D algorithm. AAPM Report No. 85 observed that air cavities presented the highest divergent values, a fact that is of clinical concern especially for tumors extending to the surface. It made several recommendations, such as: (i) scatter correction for 1D, 2D or 3D should be ascertained, and electron transport handling ability should be checked; (ii) in the vicinity of soft tissues and air cavities, superposition/convolution algorithms and MC simulation based algorithms should be considered. Later, Papanikolaou and Stathakisa^{li} published a paper describing the evolution of dose calculation algorithms in terms of their heterogeneity correction performance, as well as the current state-of-the-art. After discussing the limitations of the Hounsfield Number, or CT Number, in a TPS, they evaluated several classical algorithms, such as the RTAR and the Batho power law; the modified Sontag and Cunningham Batho method; 2D correction algorithms such as equivalent TAR (ETAR) and Fast Fourier Transforms (FFT). Most of these earlier algorithms, however, had low accuracy owing to imperfect scatter dose simulations; this limitation was overcome by implementing ray scattering in three dimensions, through algorithms such as differential scatter air ratio (DSAR) (Cunningham), delta volume (Wong and Henkelman), the dose spread array (Mackie et al.), and the differential pencil beam proposed by Mohan et al.^{li}

2. Monte-Carlo Algorithm

As computing speed increases, the Monte Carlo algorithm is becoming more widespread in a variety of applications, including PET and SPECT imaging, EPID dose conversion, dose calculation etc. While two popular algorithms for chest cavity modeling and dose calculation in IMRT are PB and collapsed cone (CC), studies have shown that MC yields superior results compared to these algorithms^{lii}. MC can better simulate maximum and mean doses and also estimates OAR values more accurately.

Simply stated, MC is a statistical technique that attempts to model an actual physical event through random number sampling. One of the earliest instances of application of the MC technique was in simulating the physical characteristics of a gamma camera – photons were tracked from their point of introduction to their point of elimination from the system^{liii}. MC estimates this path length x by sampling a probability density function (PDF) of x , and calculating a cumulative PDF (CPDF):

$$CPDF(x) = \int_0^x PDF(\zeta) d\zeta,$$

where ζ is a random variable. The variable ζ is sampled by substituting it with a random number in the range (0, 1) and calculating the value of x . Most often PDF(x) cannot be integrated using first principle, and in such cases the value of CPDF(x) is calculated using numerical methods. The stochastic nature of particle absorption and scattering is modeled by using a variety of random number generators (RNGs). One of the commonest is called the Linear Congruential RNG (LCRNG), and is described by the equation

$$X_{n+1} = a(X_n + C) \bmod(m),$$

where m is the modulus of the system, a is a multiply factor and C is a constant. The modulus m is usually assigned the value of a prime number or an exponent of 2 ^{liv}. If C is

assigned the value 0 then the generator, Multiplicative LCRNG (MLCRNG) is obtained; this variation is used in many commercial implementations. Each path calculation is called a history, and the MC algorithm converges correctly as a greater number of histories are included within the calculated volume. However, for low statistical uncertainty this also necessitates very high number of calculations, making the process slower^{lv}. Depending on the algorithm used to model transport phenomena, MC can be divided into three types: condensed history (Class I), mixed simulation (Class II), and event-by-event code^{lvi}.

There is an extensive literature commenting on MC usage in CyberKnife, as well as comparison between MC and other algorithms such as RT and Anisotropic Analytical Algorithm (AAA). A commercial MC algorithm for an IMRT planning system, the Monaco v.1.0, was investigated for dose accuracy by Grofsmid et al.^{lvii} They observed only a 2% or 2 mm distance-to-agreement between calculated dose distribution and those observed in water and tissue equivalent phantoms. However, they observed a higher difference of 6% at bone interfaces, possibly because MC calculated dose to bone. Similarly, dosimetric validation of the Acuros XB algorithm, released for external beam therapy by Varian Medical Systems, was performed by Bush et al.^{lviii} The validation was performed for lung, bone, and air against ion chamber measurement of 6 and 18 MV beam energies; calculations from standard AAA algorithm were used as reference. The Acuros XB employs a variant of MC in which a grid-based methodology is used (instead of stochastic solutions employed by conventional MC). The authors found excellent agreements between observed and calculated doses under a variety of conditions; some of the agreements were even closer than those achieved using AAA. However, they

recommended two changes: inclusion of air in the default list, because air is present in many structures that require contouring, and proper assignments of bone and cartilage values, since the Z value of cartilage is nearer to soft tissue than bone^{lvii}.

A comparison between MC and RT dose calculations for lung irradiation using CyberKnife was performed by Wilcox et al.^{iv} The authors used a PTV that was 3-5mm greater than the GTV and the dose was delivered to the PTV at the 60-80% isodose line. They observed a discrepancy of 1-2 Gy for maximum dose to critical organs such as heart, trachea, esophagus etc.; RT over-calculated the dose consistently. The highest difference was noted in case of the lung, possibly because RT over calculates in low-density material and for low collimator openings. Based on their results, the authors concluded that MC dose calculations are more effective than simple RT calculations, especially for small collimator sizes. More recently, the performance of MC at various lung-tumor interface points has also been performed. Taylor et al.^{lix} compared two variants of MC with a PBC algorithm for proximal, distal, and lateral aspects of a hypothetical tumor. They observed lower dose delivery at certain points in the periphery and recorded the ratios of doses delivered within the tumor (which can be calculated more correctly by the TPS) and those delivered at interfaces. Based on these ratios, they calculated a Dose Reduction Factor (DRF) having a mean of 0.97 for a 6 MV linac beam and 0.95 for a 15 MV linac beam. From the brief survey of literature, as presented above, it can be concluded that different versions of the MC algorithm have become a viable alternative for dose calculations in lung radiotherapy.

II. METHODS

A. Treatment plan selection

The treatment plans used in this retrospective study were created for the treatment of lung cancer patients that were treated with SBRT using the CyberKnife at Broward Health North, BHN, between November 2009 and February 2014. Plans for one hundred and two consecutive cases were analyzed to determine the feasibility of introducing the MC algorithm into clinical practice. These cases range in PTV volume from 4,017 to 175,249 mm³ (4 – 175 cc) and include PTVs located in the lung near the chest wall, surrounded by lung tissue and near the mediastinum.

B. Ray Tracing treatment plans

Historic plans were archived at the time of their creation and unarchived and examined using Multiplan treatment-planning version 8.3/4.3 for the purposes of this analysis. All the treatment plans were generated at BHN using normal breathing CT-scans of the neck, thorax, and abdomen with slice thicknesses between 1 and 2 mm with a maximum of 500 slices per study. The gross tumor volume (GTV) was delineated by the physician. The planning target volume (PTV) was generated by adding either 4 or 5 mm to the GTV, with exceptions in cases where the GTV was near organs at risk (OAR), and then individualized by the physician. A schematic based on ICRU report 62 is shown in Figure 7 giving the GTV, clinical target volume (CTV), internal target volume (ITV), and PTV as well as an OAR^{lx}. OARs were defined and contoured according to the Radiation

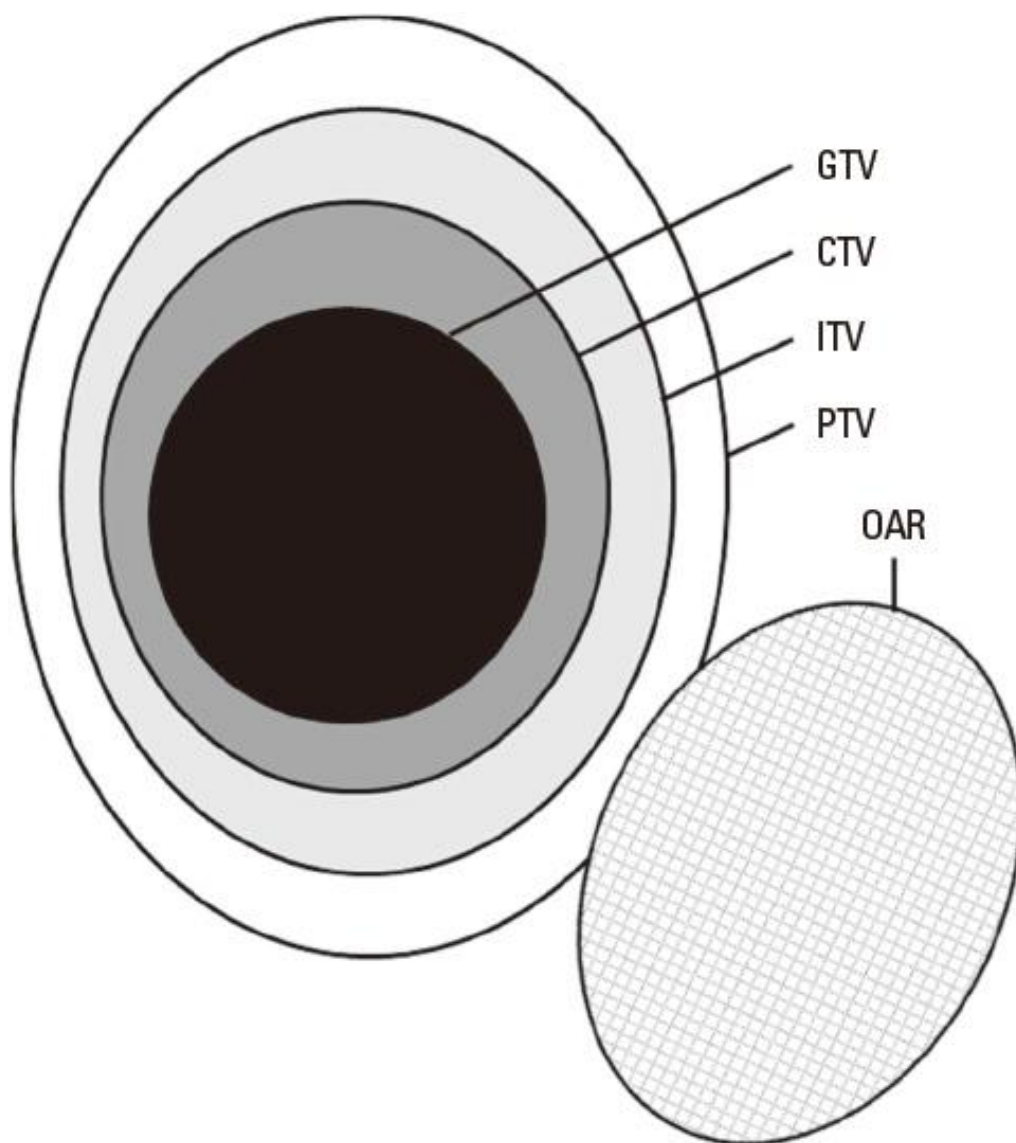


Figure 7: Schematic based on ICRU report 62 with the GTV, clinical target volume (CTV), internal target volume (ITV), and PTV as well as an OAR^{lx}.

Therapy Oncology Group (RTOG) 1106 OAR guidelines. Spinal cord, heart, esophagus, and total lung minus PTV were contoured for all cases. The trachea and ipsilateral main bronchus (92 cases), great vessels (97 cases), and ribs (20 cases) were contoured on a case-by-case basis. The historic plans were optimized and calculated using a Ray Trace high-resolution algorithm. The final calculation box was opened by the operator to

include the entire patient geometry as recorded in the CT simulation study. Prescription doses (Rx) ranged from 18 to 60 Gy (1800 to 6000 cGy) and the number of treatments ranged from 2 to 5 treatments per case. The dose prescription isodose line was determined by the physician and ranged between 70 to 90%, which followed the general guidelines that the prescription isodose line should cover at least 95% of the PTV^{lxi}.

C. Monte Carlo treatment plans

For each of the 102 historic plans, a second plan was generated. These new treatment plans were recalculated using the MC algorithm, but not re-optimized. The uncertainty of the MC calculation was set to 1% and a high-resolution grid (512^2) was used. For the MC calculation, the dose is generated based on the full patient geometry by default^{xxxiii}. The collimator size, the number of beams, and the monitor units were kept unchanged from the original RT plans. The prescription for each plan was not renormalized. A comparison of isodose distribution on a CT-scan for an RT calculated plan (left) and an MC calculated plan (right) is shown in Figure 8. Note- the RT calculated plan is overestimating the dose delivered to the PTV, as compared to the MC calculated plan.

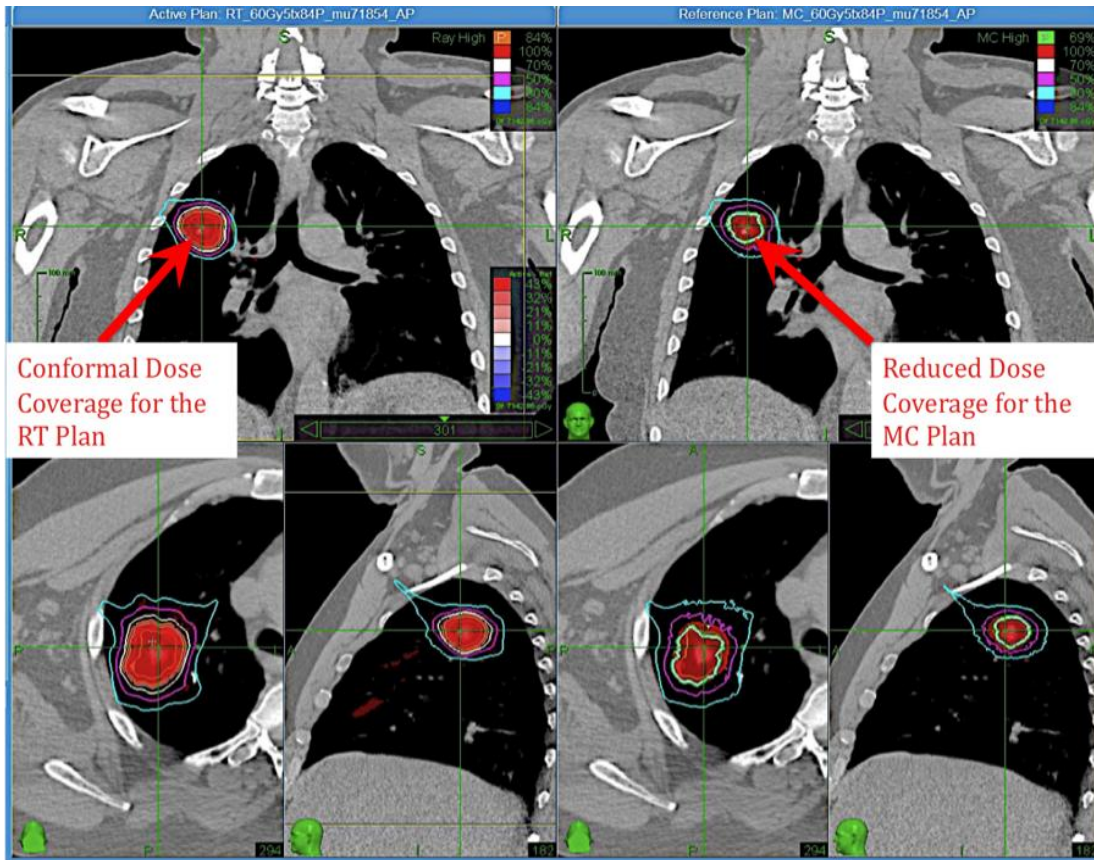


Figure 8: CT-Scan showing differences in PTV between RT and MC calculated plans.

D. Data Analysis

The data collection was obtained through use of the graphical and tabular dose volume histogram (DVH) tool in the Multiplan software and recorded and analyzed using Microsoft® Excel® 2008 for Mac version 12.3.5. As example, Figure 9 shows the graphical and tabular DVH for a lung treatment plan. In the graphical DHV, solid lines were the result of the RT algorithm calculation while dashed lines were from the MC algorithm.

Recorded dose parameters include the GTV and PTV volumes, as well as the mean, minimum, and maximum doses (D_{mean} , D_{min} , and D_{max} , respectively) for those



Figure 9: Graphical DVH (top) comparison between the RT and MC calculations and tabular DVH (bottom) for the historic RT calculated plan.

volumes and the doses that cover 99%, 95%, and 1% (D99, D95, and D1, respectively) of the volumes (in cGy). The DVH curves in Figure 9 show the percentage of volume (along the y-axis) of a structure (such as GTV, PTV or an OAR) that receives a dose. Dose increases toward the right along the x-axis. The dose parameters are found along these curves in the following order from upper left to lower right: Dmin, D99, D95, Dmean, D1, and Dmax. The volume of lung tissue (air density equivalent) inside the PTV is used to calculate the “air in PTV” ratio (APR), the ratio of the volume of lung tissue inside the PTV to the PTV. The prescription isodose volume (mm³), the 50% prescription isodose volume (mm³), and the maximum dose (cGy) of the dose prescribed

at 2 cm from the PTV in any direction, were collected to calculate conformity parameters to compare with RTOG 0813 and 0915 protocol criteria. These include the Conformality Index (CI), which is the ratio of the prescription isodose volume to PTV, the ratio of the 50% prescription isodose volume to PTV (R50%), and the maximum dose (%) at 2 cm from PTV in any direction (D2cm). RTOG standard protocol values for these parameters are included in Table III.

In order to analyze how the MC calculation dose differs from the RT calculation for the OARs in the thoracic cavity, the maximum dose (in 30 mm³ of volume) in the

Table III: RTOG Protocols.

| PTV Volume (cc) | Ratio of Prescription Isodose Volume to the PTV Volume, CI | | Ratio of 50% Prescription Isodose Volume to the PTV Volume, R _{50%} | | Maximum Dose (in % of dose prescribed) @ 2cm from PTV in Any Direction, D _{2cm} (Gy) | |
|--------------------|--|-------|--|-------|--|--------|
| | Deviation | | Deviation | | Deviation | |
| | None | Minor | None | Minor | None | Minor |
| 1.8 | < 1.2 | < 1.5 | < 5.9 | < 7.5 | < 50.0 | < 57.0 |
| 3.8 | < 1.2 | < 1.5 | < 5.5 | < 6.5 | < 50.0 | < 57.0 |
| 7.4 | < 1.2 | < 1.5 | < 5.1 | < 6.0 | < 50.0 | < 58.0 |
| 13.2 | < 1.2 | < 1.5 | < 4.7 | < 5.8 | < 50.0 | < 58.0 |
| 22.0 | < 1.2 | < 1.5 | < 4.5 | < 5.5 | < 54.0 | < 63.0 |
| 34.0 | < 1.2 | < 1.5 | < 4.3 | < 5.3 | < 58.0 | < 68.0 |
| 50.0 | < 1.2 | < 1.5 | < 4.0 | < 5.0 | < 62.0 | < 77.0 |
| 70.0 | < 1.2 | < 1.5 | < 3.5 | < 4.8 | < 66.0 | < 86.0 |
| 95.0 | < 1.2 | < 1.5 | < 3.3 | < 4.4 | < 70.0 | < 89.0 |
| 126.0 | < 1.2 | < 1.5 | < 3.1 | < 4.0 | < 73.0 | < 91.0 |
| 163.0 | < 1.2 | < 1.5 | < 2.9 | < 3.7 | < 77.0 | < 94.0 |

spinal cord, esophagus, heart, great vessels, trachea and ipsilateral main bronchus, and ribs, and the dose for 5000 mm³ of the esophagus and for 15000 mm³ of the heart (all in cGy), the volume of the total lungs minus PTV (in mm³) receiving doses of 500, 1000, and 2000 cGy and the dose (in cGy) for 1500 and 1000 cc of total lung minus PTV were recorded.

E. Statistics

Statistical approaches were used to determine the statistical significant effects of changing the treatment-planning algorithm from RT to MC. Dependent sample t-tests were used with the dose parameters (Dmin, D99, D95, Dmean, D1, and Dmax) for both GTV and PTV to test the null-hypothesis that there is no difference in the average value of these parameters between the RT and MC calculated plans. After dividing the dose parameters into PTV size regimes, a Kruskal-Wallis test was used to determine if the effect of changing the algorithm was significantly affected by the size of the tumor. The parameters were divided into three PTV regimes, less than 20,000 mm³, greater than 20,000 to 50,000 mm³, and greater than 50,000 mm³. Alternatively, the dose parameters were also divided into regimes based on the APR ratio, with regimes of < 50%, greater than 50% to 70%, and greater than 70% and the Kruskal-Wallis test was recalculated for the dose parameters for these APR regimes as well. Spearman rank correlations were also calculated for the dose parameters as well as for the RTOG protocol criteria. Dependent sample t-tests were also conducted for the OAR parameters. All tests were two-sided with a significance level of $\alpha = 0.05$.

III. RESULTS

Previous studies have shown that doses calculated by the MC algorithm are smaller in general as compared to the RT algorithm. These differences are related to the methods used for each algorithm. The RT algorithm dose is calculated by applying an equivalent path length correction without factoring in the effect of lateral electron disequilibrium. On the other hand, the MC algorithm calculations provide accurate dose distributions for heterogeneous patient geometries and complex beam delivery configurations^{xxxiii, lxii}. Thus the MC algorithm is considered more accurate than the RT algorithm, especially in regions of high heterogeneity or when tumors are small^{xlv}. These differences in algorithms were also shown to significantly affect the Conformality Index (CI) and the ratio of the 50% isodose to the PTV (R50%) as well.

A. Dose parameters (target coverage)

In order to quantify the effect of tissue heterogeneities on the dose calculations from the RT and MC algorithms, the mean for each of the recorded dose parameters (Dmin, D99, D95, Dmean, D1, and Dmax for GTV and PTV) was calculated for all 102 plans for each algorithm. These means are given in Table IV. T-tests determined that there was a significant difference between the algorithm means for all of these dose parameters. The p-values for each test are also included in Table IV.

Table IV: T-test results for GTV and PTV Dose Parameters. All tests are two-tailed and with a significance level of $\alpha = 0.05$.

| Dose Parameter (cGy) | p-value | RT Mean | MC Mean | (MC – RT) / RT (%) |
|----------------------|----------|---------|---------|--------------------|
| GTV: | | | | |
| Dmin | 1.2 E-28 | 5060 | 3756 | -25.77 |
| D99 | 2.3 E-24 | 5256 | 4255 | -19.05 |
| D95 | 1.6 E-25 | 5414 | 4527 | -16.37 |
| Dmean | 9.1 E-30 | 5832 | 5134 | -11.98 |
| D1 | 4.6 E-27 | 6241 | 5710 | -8.50 |
| Dmax | 6.8 E-21 | 6321 | 5872 | -7.10 |
| PTV: | | | | |
| Dmin | 3.2 E-33 | 4558 | 2962 | -35.00 |
| D99 | 2.8 E-31 | 4977 | 3532 | -29.03 |
| D95 | 2.7 E-28 | 5204 | 3830 | -26.40 |
| Dmean | 1.9 E-22 | 5781 | 4785 | -17.22 |
| D1 | 9.8 E-28 | 6228 | 5681 | -8.77 |
| Dmax | 1.4 E-19 | 6333 | 5902 | -6.81 |

The normalized difference between the MC algorithm and the RT algorithm was then found for each dose parameter by taking the MC algorithm calculated value minus the RT algorithm calculated value and then dividing this difference by the RT algorithm value. This normalized difference is expressed as a percent change from the RT value to the MC value, and listed in the last column of Table IV. For the GTV dose parameters, the change from RT to MC ranged from a decrease of 7.1% for Dmax to a decrease of 25.77% for Dmin. For the PTV dose parameters, the change from RT to MC ranged from a decrease of 6.81% for Dmax to a decrease of 35.00% for Dmin. Overall, the

decrease between algorithms was greater for the PTV dose parameters. Only Dmax had a greater change between the algorithms for GTV than for PTV. As compared to the RT calculated plans, on average, the PTV D99 was more than 29% lower for the MC calculated plans, the PTV D95 was more than 26% lower for the MC calculated plans, the PTV D1 was more than 8% lower for the MC calculated plans, and the PTV Dmean was more than 17% lower for the MC calculated plans.

For each of the dose parameters, a percent change between the RT algorithm calculated value and the MC algorithm calculated value for each individual plan was also calculated for both GTV and PTV. The individual percent changes for the GTV dose parameters (D99, D95, Dmean, and D1 only) are plotted versus GTV in Figures 10 through 13, respectively, and the individual percent changes for the PTV dose parameters (D99, D95, Dmean, and D1 only) are plotted versus PTV in Figures 14 through 17, respectively. Dmax and Dmin are excluded, as they are not considered to be clinically relevant. Results for both the GTV and PTV dose parameters are shown subdivided into regimes based on plan PTV volume, with those plans with a volume of less than 20,000 mm³ in one regime, those with a volume between 20,000 and 50,000 mm³ in second regime, and those a volume of greater than 50,000 mm³ in a third. Although these regimes were chosen arbitrarily in an attempt to evenly distribute the data, it was found these regimes well delineated the maximum values found in the data for each regime (see figures 14 and 15, for instance).

The individual plan percent changes were negative (indicating the dose parameter value was smaller for the MC algorithm calculated value) for nearly all of the shown dose parameters, though there were at least some plans close to zero for all dose parameters.

Positive percent changes were recorded for only D1 and D95 for GTV (2 plans and 1 plan, respectively) and only for D1 for PTV (2 plans) and all of these positive changes were less than 1%. For all dose parameters shown in Figures 10 through 17, the largest percent changes were found in the regime containing the plans with the smallest PTV volume. Nonetheless, for each dose parameter, this regime also included plans with percent changes that were close to zero. Thus, this regime also contained the largest variability. As the GTV or PTV increased, both the variability and the overall difference between the algorithms decreased for all dose parameters. For both the GTV and the PTV dose parameters, D99 and D95 had greater percent changes for the individual plans than Dmean or D1. For GTV, the maximum percent change for D99 and D95 was around a 55-60% decrease, while Dmean and D1 maximum changes were around a 25-30% decrease. For PTV, the maximum percent change for D99 was around a 70% decrease and for D95 was around 90%. Dmean was around a 50% decrease, while D1 had a maximum change of around 30%.

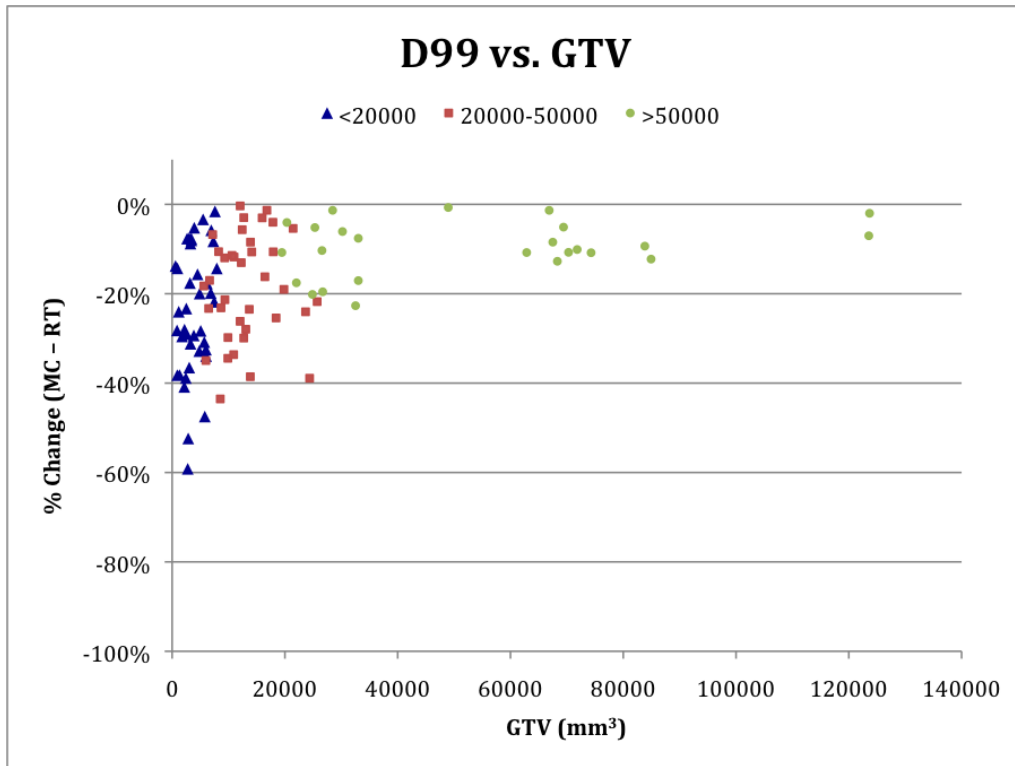


Figure 10: D99 versus GTV.

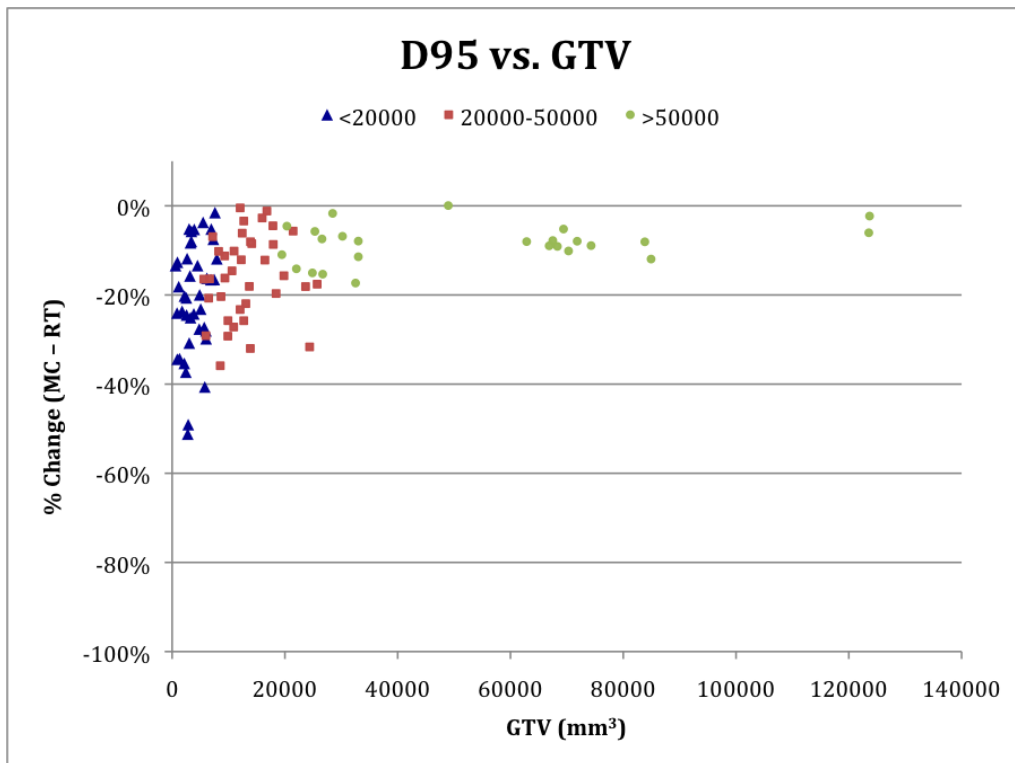


Figure 11: D95 versus GTV.

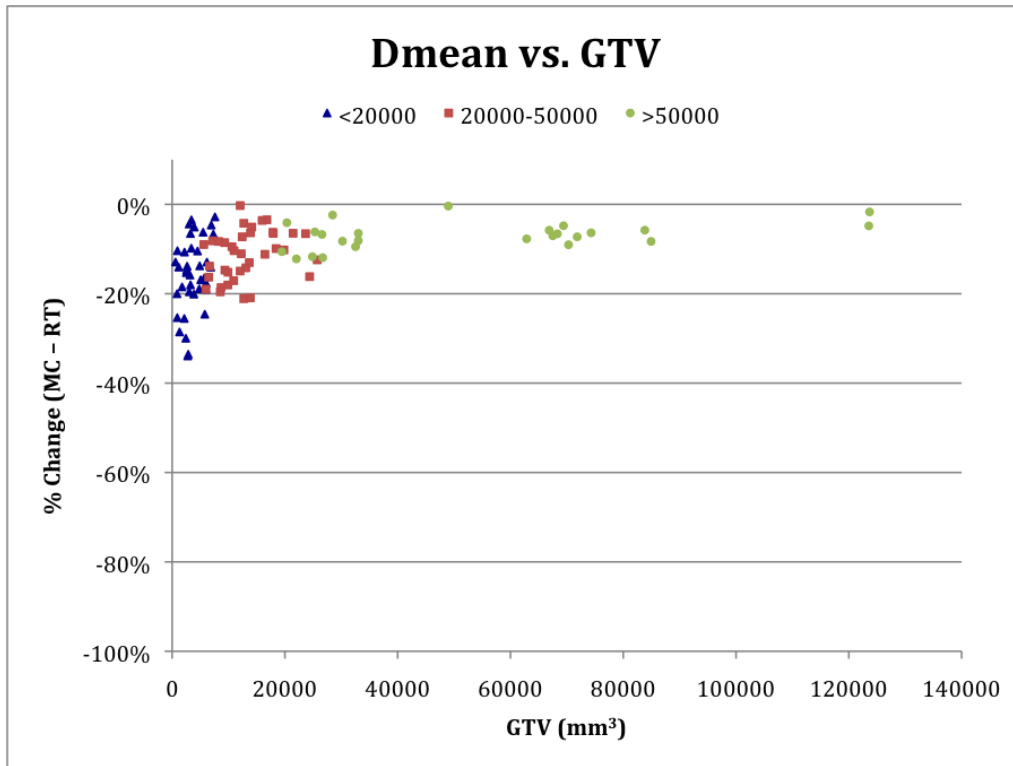


Figure 12: Dmean versus GTV.

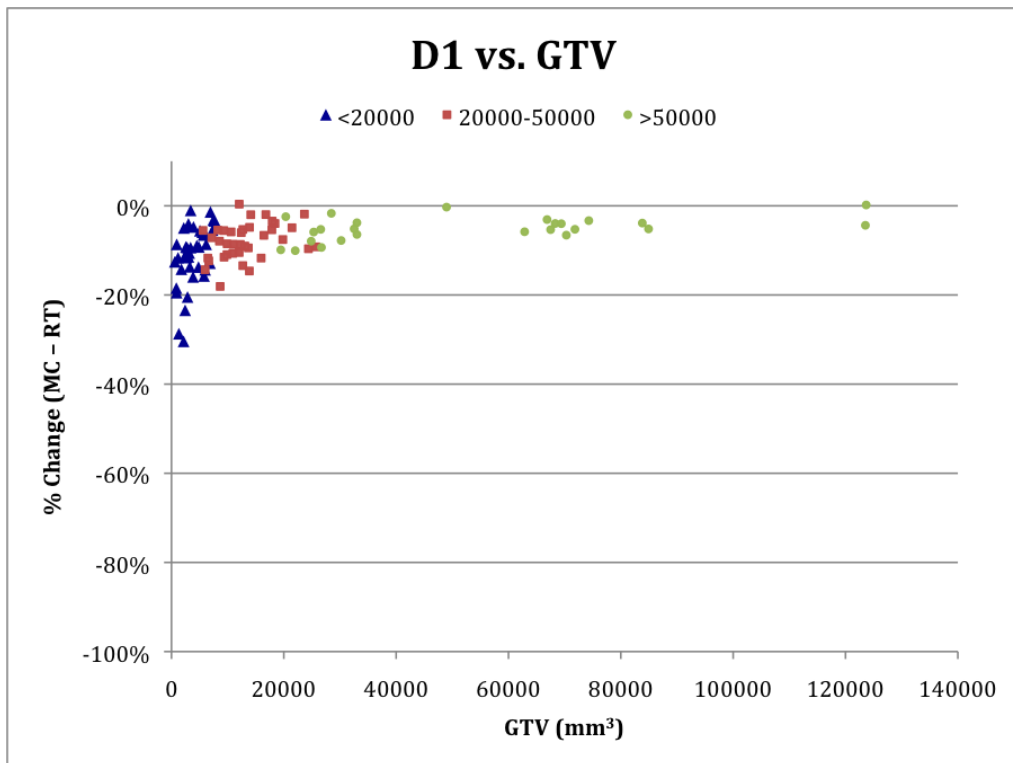


Figure 13: D1 versus GTV.

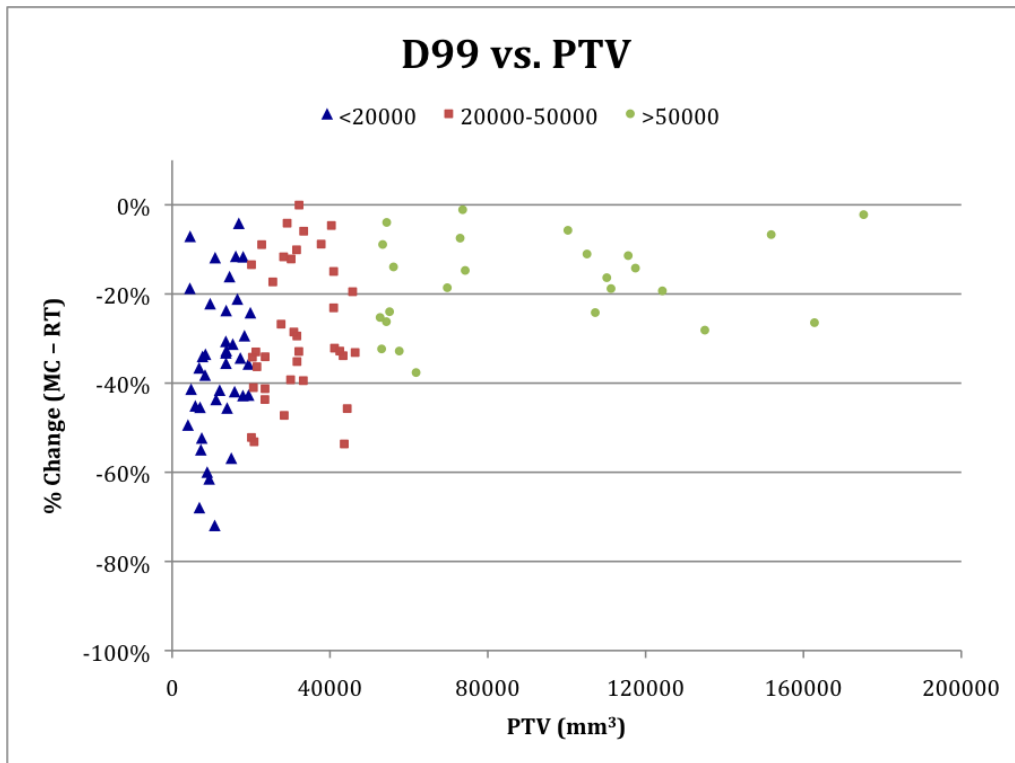


Figure 14: D99 versus PTV.

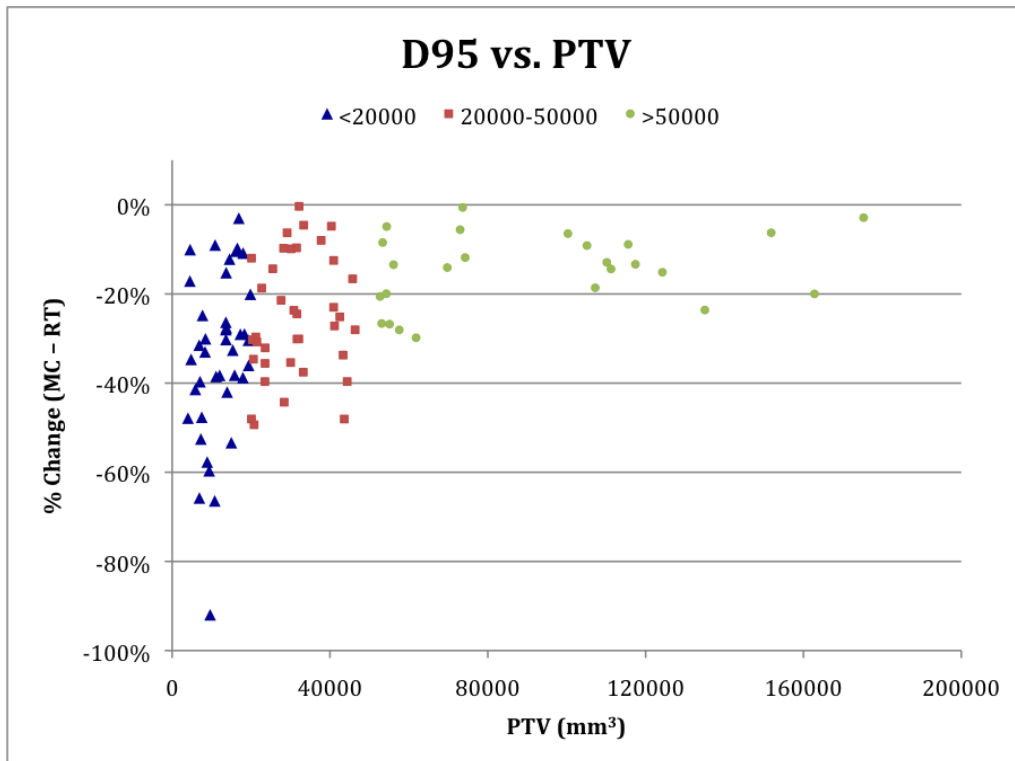


Figure 15: D95 versus PTV.

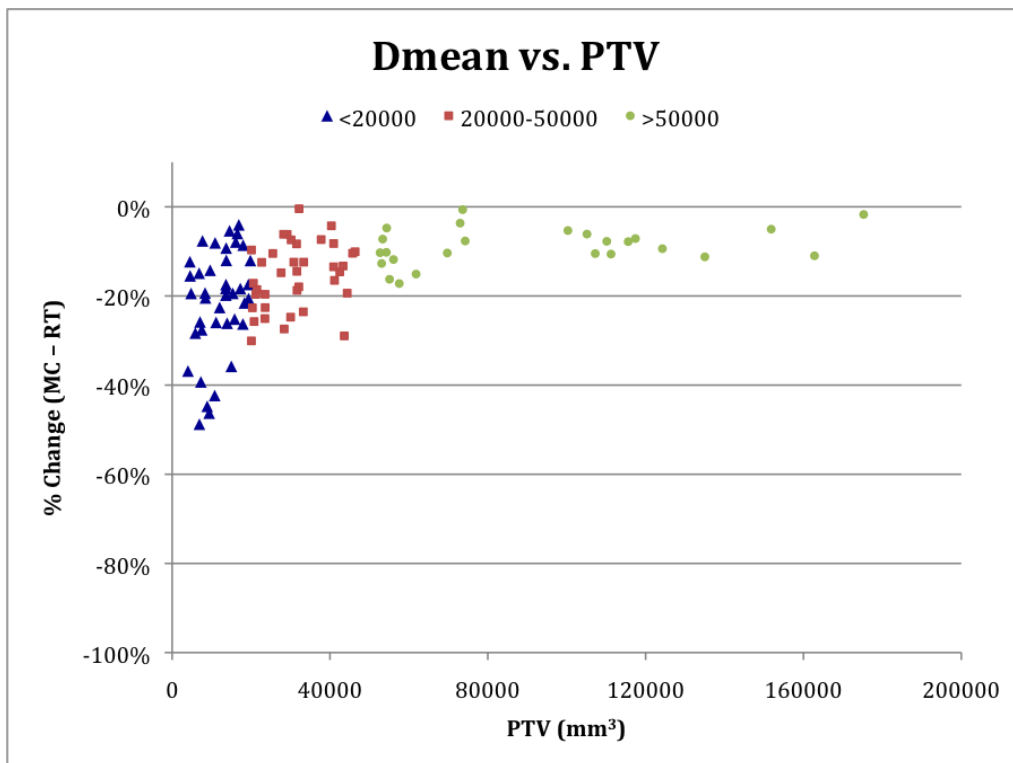


Figure 16: Dmean versus PTV.

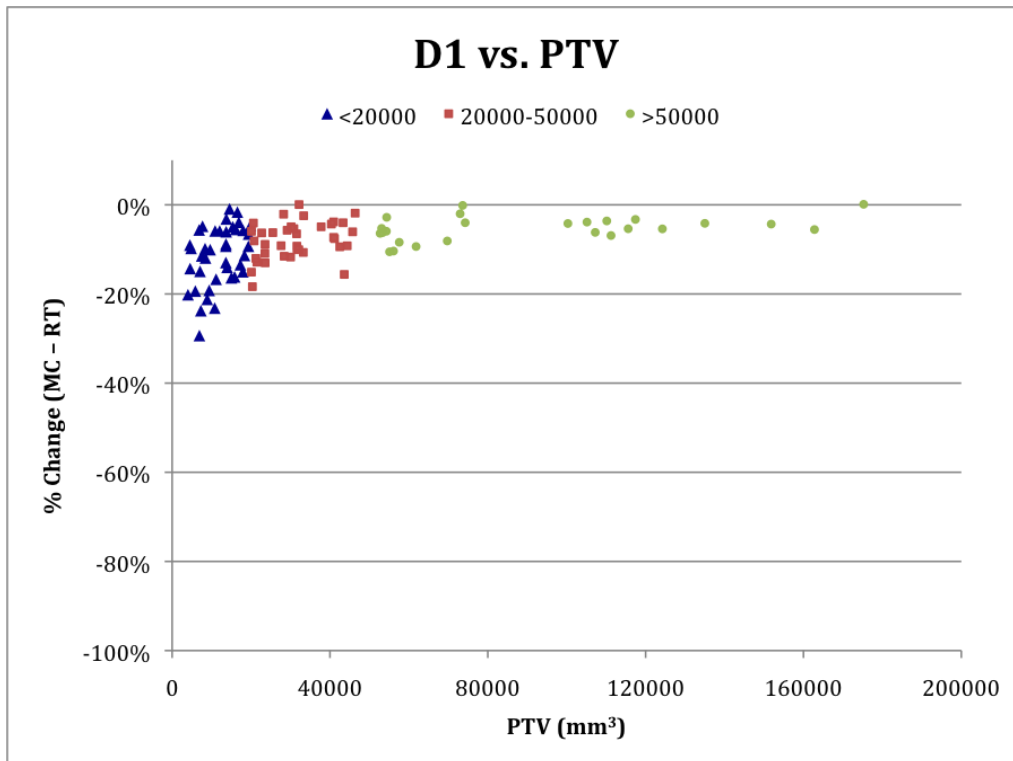


Figure 17: D1 versus PTV.

Two statistical tests were used to determine the significance of the percent changes in each dose parameter for the individual plans resulting from the change in the algorithm and their relationship with the change in PTV Volume. First, correlations, including Spearman Rank correlations, were calculated and the correlation coefficients were found. The coefficients for all of the dose parameters are given in Tables V and Spearman Rank correlation coefficients are given for the PTV dose parameters D99, D95, Dmean, and D1 in Table VI. Second, the Kruskal-Wallis test was used to determine if significant differences exist between the 3 PTV volume regimes. These values are given in Table VII.

Table V: Correlations of Treatment Plan Dose Parameters with GTV, PTV, and APR.

| Dose Parameter | Correlation of Dose Parameters with GTV | Correlation of Dose Parameters with PTV | Correlation of Dose Parameters with APR |
|----------------|---|---|---|
| GTV: | | | |
| Dmin | 0.273 | 0.286 | -0.462 |
| D99 | 0.383 | 0.417 | -0.501 |
| D95 | 0.385 | 0.420 | -0.532 |
| Dmean | 0.423 | 0.456 | -0.635 |
| D1 | 0.401 | 0.425 | -0.621 |
| Dmax | 0.488 | 0.501 | -0.598 |
| PTV: | | | |
| Dmin | 0.332 | 0.365 | -0.442 |
| D99 | 0.428 | 0.435 | -0.513 |
| D95 | 0.417 | 0.444 | -0.502 |
| Dmean | 0.443 | 0.472 | -0.614 |
| D1 | 0.417 | 0.444 | -0.640 |
| Dmax | 0.485 | 0.505 | -0.563 |

Table VI: Spearman Rank Correlations for Selected Dose Parameters.

| Dose Parameter | Correlation of Dose Parameters with PTV | Correlation of Dose Parameters with APR |
|----------------|---|---|
| PTV: | | |
| D99 | 0.499 | -0.547 |
| D95 | 0.517 | -0.571 |
| Dmean | 0.542 | -0.665 |
| D1 | 0.502 | -0.680 |

Table VII: Kruskal-Wallis Test Statistics for Selected Dose Parameters.

| PTV Dose Parameter | Regime 1 Mean | Regime 2 Mean | Regime 3 Mean | Test Statistic (H) | p-value |
|--------------------|------------------------------------|--|------------------------------------|--------------------|---------|
| vs. PTV (N = 102): | < 20000 mm ³ (40 cases) | 20001-50000 mm ³ (37 cases) | > 50000 mm ³ (25 cases) | | |
| D99 | 59830 | 100048 | 132165 | 34.179 | 3.8E-08 |
| D95 | 56927 | 96952 | 136900 | 23.129 | 9.5E-06 |
| Dmean | 57078 | 92700 | 142884 | 25.280 | 3.2E-06 |
| D1 | 60918 | 101091 | 123622 | 17.249 | 1.8E-04 |
| vs. APR (N = 96): | < 0.50 (28 cases) | 0.50 - 0.70 (42 cases) | > 0.70 (26 cases) | | |
| D99 | 116033 | 105902 | 23161 | 34.495 | 3.2E-08 |
| D95 | 123292 | 97345 | 23161 | 23.171 | 9.3E-06 |
| Dmean | 138604 | 96193 | 17576 | 34.222 | 3.7E-08 |
| D1 | 141290 | 100060 | 14642 | 38.886 | 3.6E-09 |

The dose parameters were correlated with plan GTV and PTV values and the magnitude of the coefficients ranged from 0.3 to 0.5 for most parameters with the less clinically significant Dmin and Dmax at either extreme of that range. The coefficients for all dose parameters were greater for the correlations with the plan PTV volume than for the correlations with GTV volume, though by no more than 2-3 hundredths. The PTV dose parameter correlation coefficients were also mostly greater than for the GTV dose parameters. The Spearman Rank correlations, given in Table VI, were only calculated for the PTV dose parameters of D99, D95, Dmean and D1. The correlations were found to be slightly stronger than the standard correlations for these parameters, with coefficients around 7 hundredths greater.

The Kruskal-Wallis test was used to determine if there existed a significant difference in the dose parameters between the PTV volume regimes shown in Figures 10 through 17. The null hypothesis was that there is no difference between the groups and based on $\alpha = 0.05$ and 2 degrees of freedom, this hypothesis was rejected when the test statistic was greater than 5.99. For all of the dose parameters, the null hypothesis was rejected indicating the size of the PTV did have a significant effect on the change of the parameter value between the two algorithms. The test statistic value was 34.18, 23.13, 25.28, and 17.25 for D99, D95, Dmean and D1, respectively.

B. Air to PTV Ratio (APR)

Additional analyses compare the percent changes in the dose parameters to the ratio of the volume of lung tissue inside the PTV to the PTV (APR), as an alternative to the comparisons to the PTV volume. For each plan, the APR was calculated, and in Figures 18 through 21, the PTV dose parameters (D99, D95, Dmean and D1),

respectively, are plotted versus the APR. As with the Figures 10 through 17 for GTV and PTV, the plans are subdivided into regimes. For APR, the subdivisions are based on APR %, with the 1st regime containing APR values less than 50%, the 2nd containing values between 50% and 70%, and the 3rd containing values greater than 70%.

For the parameters plotted versus APR, the largest percent changes between the algorithms were found when the APR approached 100% and while the smallest percent changes were when the APR was less than 50%. Furthermore, unlike the dose parameter percent changes plotted versus GTV and PTV, there appeared to be fewer instances of plans with percent changes near zero in the regime that also contained the largest percent changes.

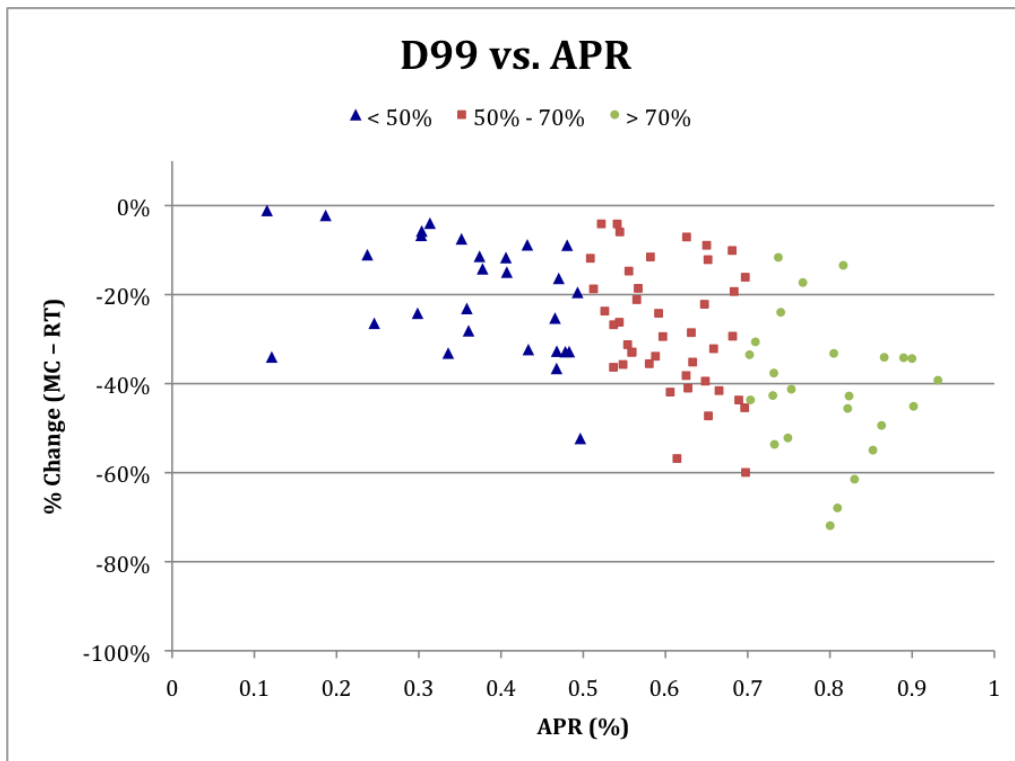


Figure 18: D99 versus APR.

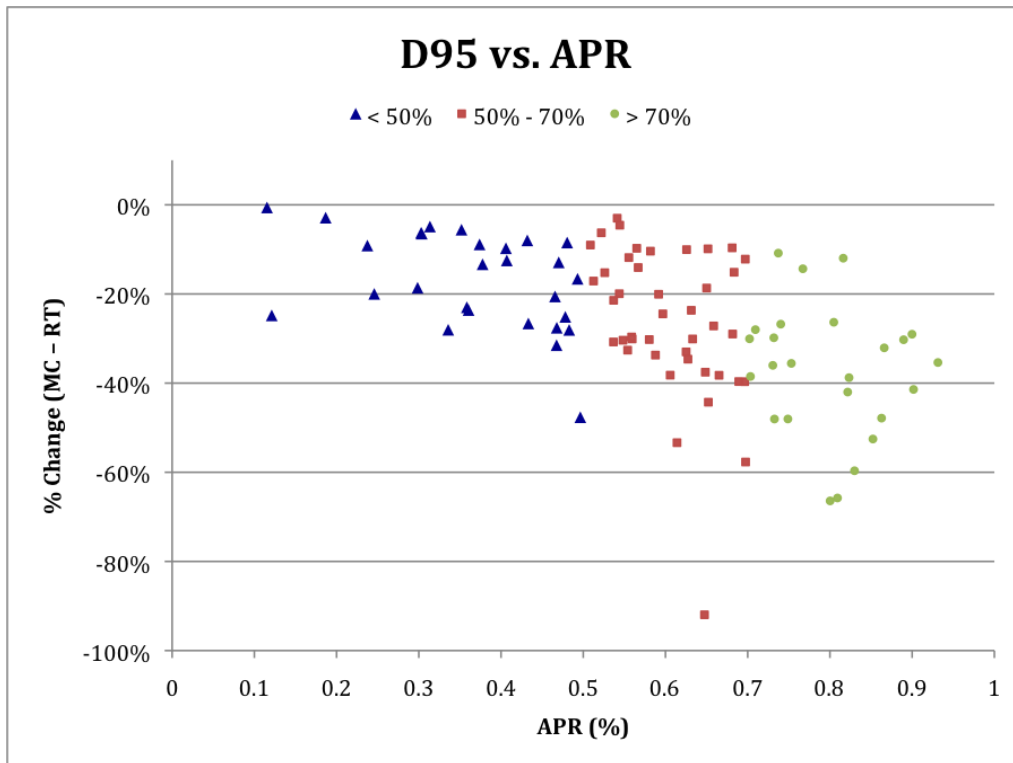


Figure 19: D95 versus APR.

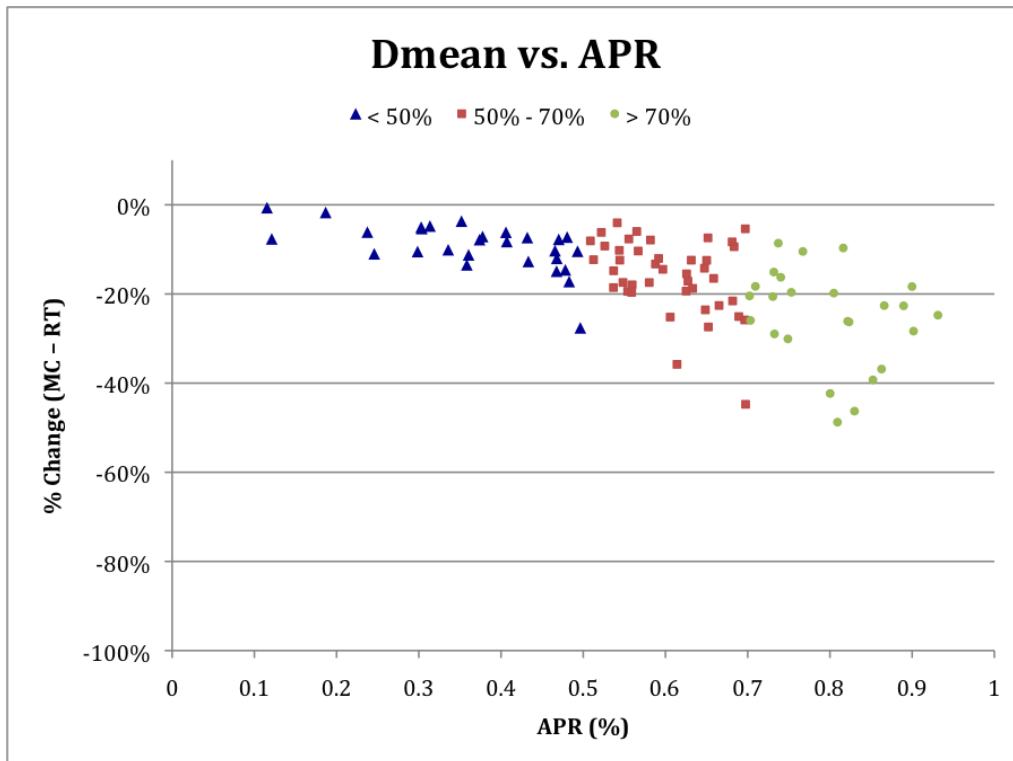


Figure 20: Dmean versus APR.

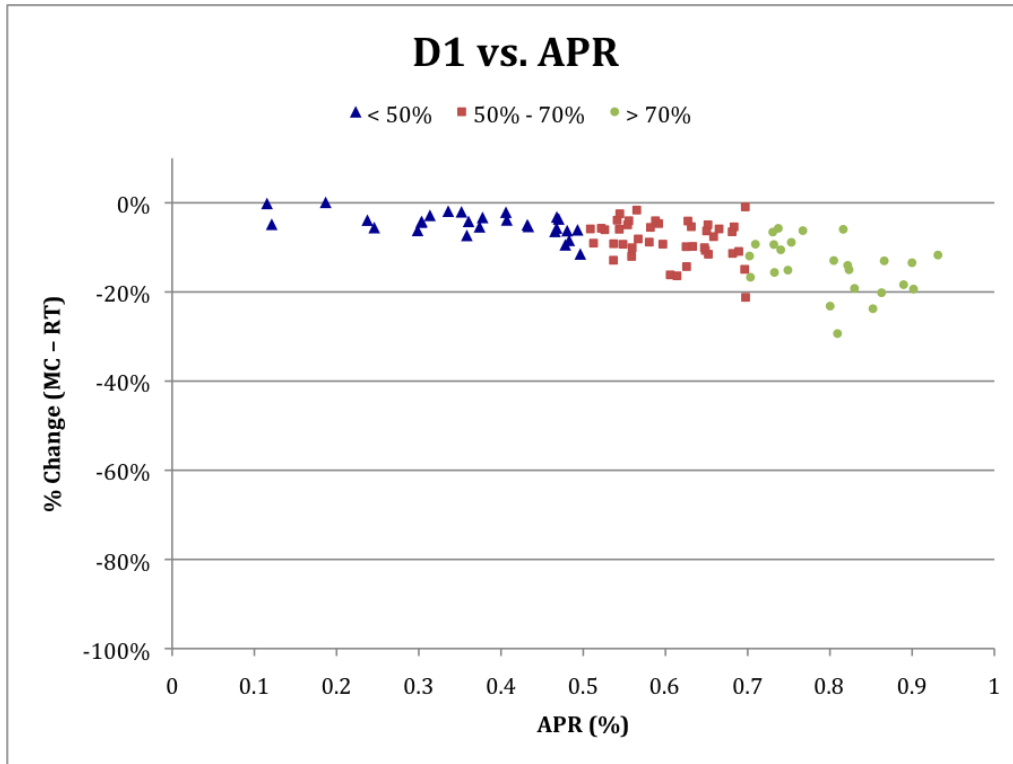


Figure 21: D1 versus APR.

The correlation analysis and Kruskal-Wallis tests were repeated for the APR data and the results are included in Tables V, VI and VII. The magnitudes of the correlation coefficients were larger for all dose parameters (both GTV and PTV) with APR when compared to the coefficients for either GTV or PTV. The largest increases in magnitude were for the GTV dose parameters, but the magnitudes of the coefficients for all parameters increased anywhere from .08 to .20. Largest increases were for the GTV and PTV Dmean and D1. Increases in the magnitude of the coefficients were also found in the Spearman Rank correlations were increases in coefficient magnitude ranged from .05 to .18 with Dmean and D1 showing the greatest increases in correlation.

The Kruskal-Wallis analysis performed using the APR percentage regimes produced similar results to the analysis performed using the PTV volume regimes for the

PTV D99 and D95 dose parameters. For Dmean and D1, the test statistic value increased substantially, especially for D1 where the statistic changed from 17.25 to 38.89. For each parameter, the test showed there was a significant difference in parameter values based on the APR.

It is known that the probability of local tumor control may be affected by differences between planned and actual delivered doses.⁶² RTOG allows for planned doses to be reported as calculated from multiple algorithms, including RT and MC. For Cyberknife, van Zyp found that doses of 3 x 20 Gy for RT ranged in equivalent MC doses from 3 x 16 Gy for tumors < 3 cm to 3 x 18 Gy for tumors > 5 cm.⁴⁶ In order to calculate equivalent doses for the cases included in the present study, the biological equivalent dose (BED) for each plan and algorithm was calculated using the linear quadratic model. Normalized differences between the values for each plan, expressed as a percent change, were then calculated. The percent changes for the individual plans were then subdivided into the APR regimes described above. The mean for the percent changes for all plans was -12.1% and was -6.1% for the 0-50% regime, -11.5% for the 50-70% regime and -19.8% for the 70-100% regime, with individual plan differences ranging from 0 to -44.6%.

C. RTOG Protocol Criteria

The Conformality Index (CI) (found by dividing the prescription isodose volume (mm^3) by the PTV), the 50% prescription isodose volume (mm^3), and the maximum dose (cGy) of the dose prescribed at 2 cm from the PTV in any direction, were collected to compare with RTOG 0813 and 0915 protocol criteria for both RT and MC algorithm

calculated plans. Similar to the dose parameter analysis, the analysis of the RTOG protocols includes comparing the RT and MC calculated means for the parameters and using a t-test to determine if the means are statistically different, which are given in Table VIII.

The results indicate that there is a significant difference between the two algorithms for both the ratio of the prescription isodose volume to PTV (CI) and the ratio of the 50% prescription isodose volume to PTV (R50%). The decrease in the mean CI for the MC calculated plans versus the RT calculated plans is more than 47% and the decrease in R50% is nearly 24%. The difference in the maximum dose (%) at 2 cm from PTV in any direction (D2cm) was also technically significant, but only weakly so. Furthermore, the actual difference between the algorithms is minor as well (around a 2% decrease from the RT to the MC algorithm).

The individual plan values for CI, R50% and D2cm for each algorithm are plotted versus PTV in Figures 22-24, respectively. Also included in the figures are linear interpolations of the RTOG protocols given in Table III for each parameter.

Table VIII: RTOG Protocol Values: T-test and Correlations.

| RTOG Protocol Values | p-value | RT Mean | MC Mean | % Change (MC – RT) | Correlation with PTV | Correlation with APR |
|----------------------|---------|---------|---------|--------------------|----------------------|----------------------|
| CI | 1.4E-31 | 1.270 | 0.669 | -47.2 | 0.345 | -0.434 |
| R _{50%} | 1.7E-15 | 3.459 | 2.634 | -23.8 | 0.344 | -0.311 |
| D _{2 cm} | 1.1E-02 | 44.664 | 43.370 | -2.9 | 0.257 | -0.103 |

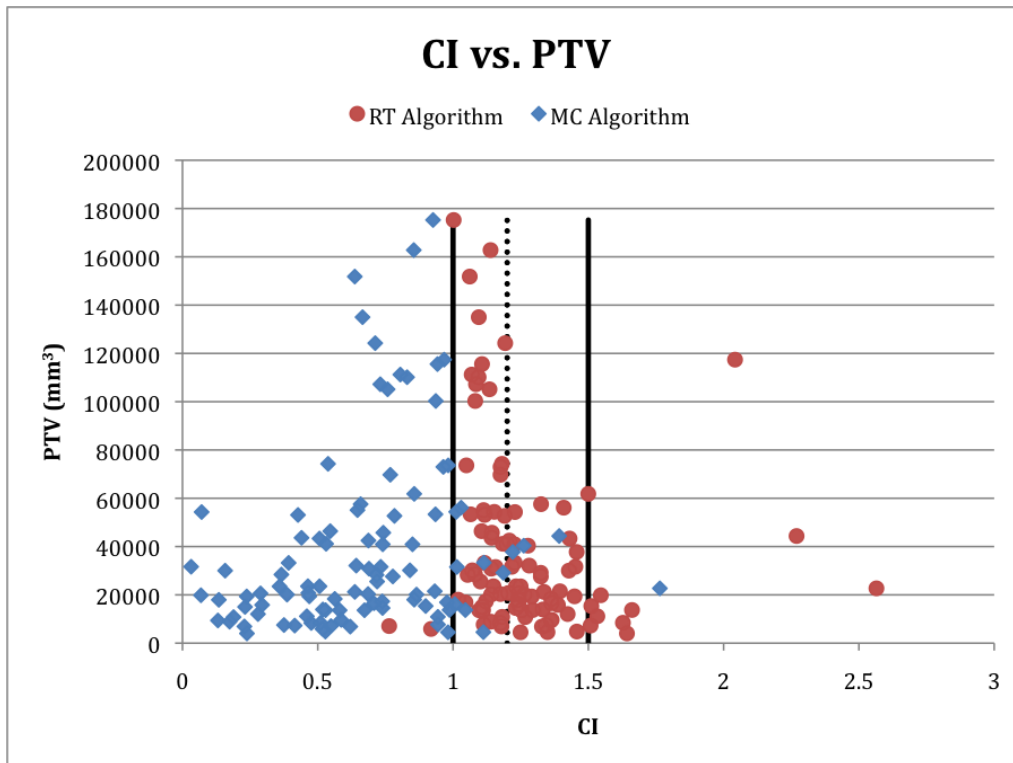


Figure 22: RTOG Protocols: CI versus PTV.

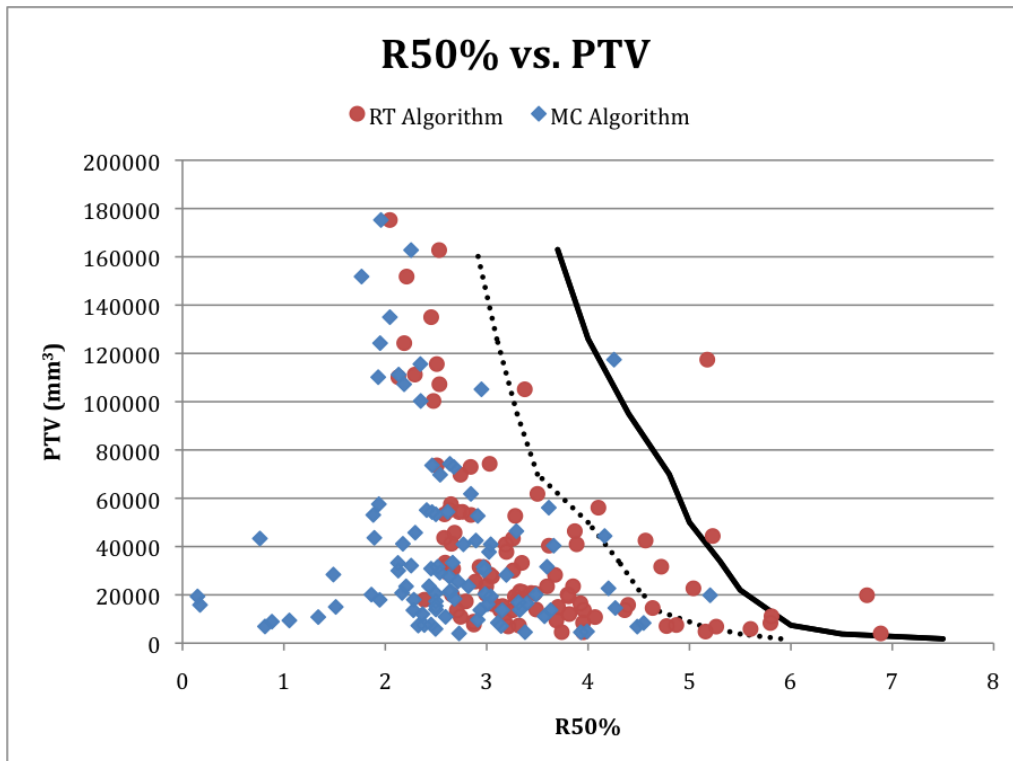


Figure 23: RTOG Protocols: R50% versus PTV.

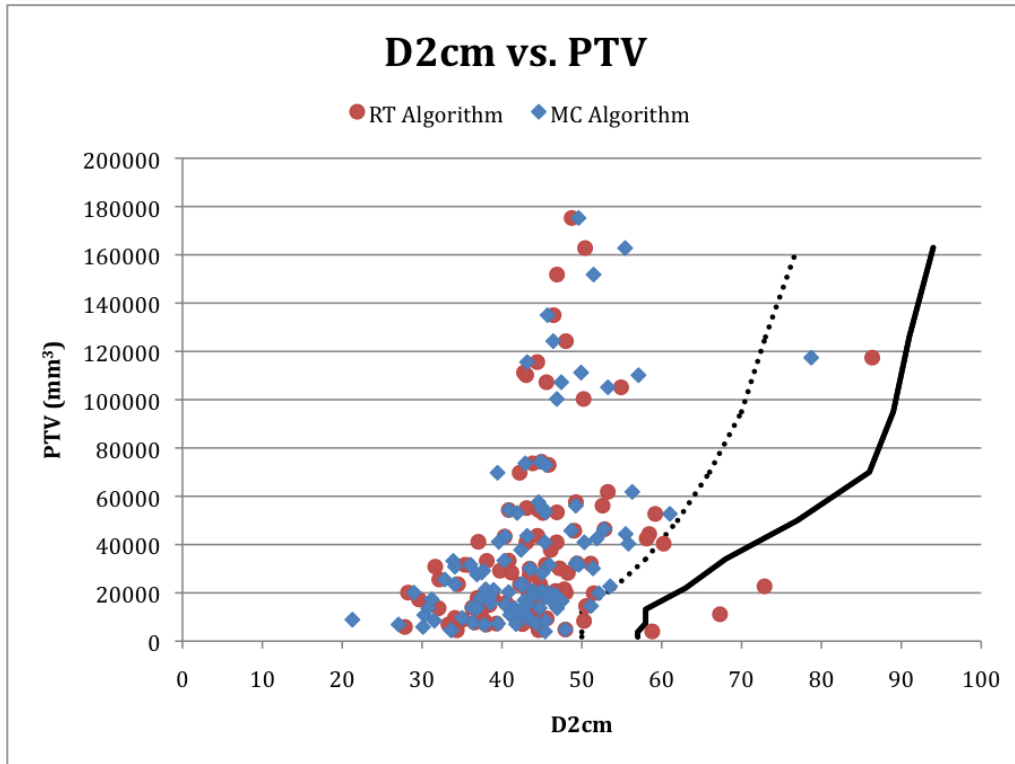


Figure 24: RTOG Protocols: D2cm versus PTV.

The individual plan values were also plotted versus APR in Figures 25-27. The protocol values for CI from Table III, which are constant, were included for Figure 25, but since no protocol values exist from RTOG for APR, no protocol values are included for Figures 26 or 27. Figure 22 shows an obvious shift toward zero in plan CI values from the RT calculated plans to the MC calculated plans plotted versus PTV. A shift is also apparent for R50% in Figure 23, though it is less pronounced than for CI, and no shift is present for the D2cm in Figure 24. The graphs for the parameters versus APR are similar to those versus PTV, though there appears to be a stronger relationship between the plan CI values versus APR for the MC algorithm in Figure 25, with the lower APR values for MC are concentrated closer to 1. The RT algorithm values, on the other hand, are spread across a wide range of APR values.

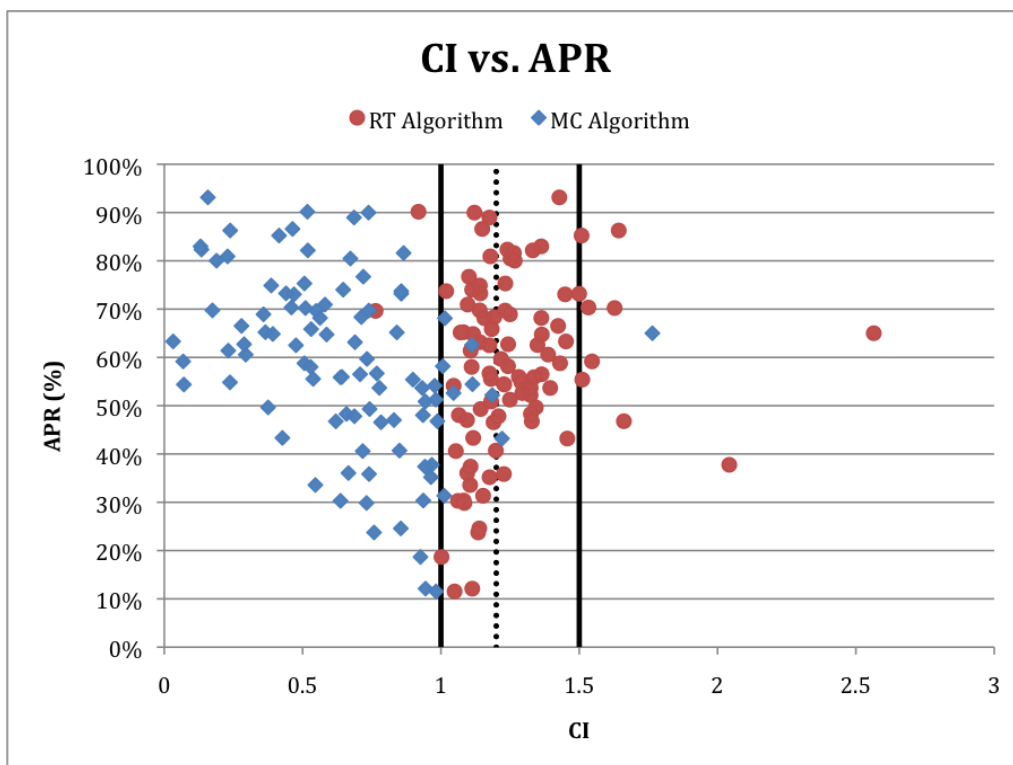


Figure 25: RTOG Protocols: CI versus APR.

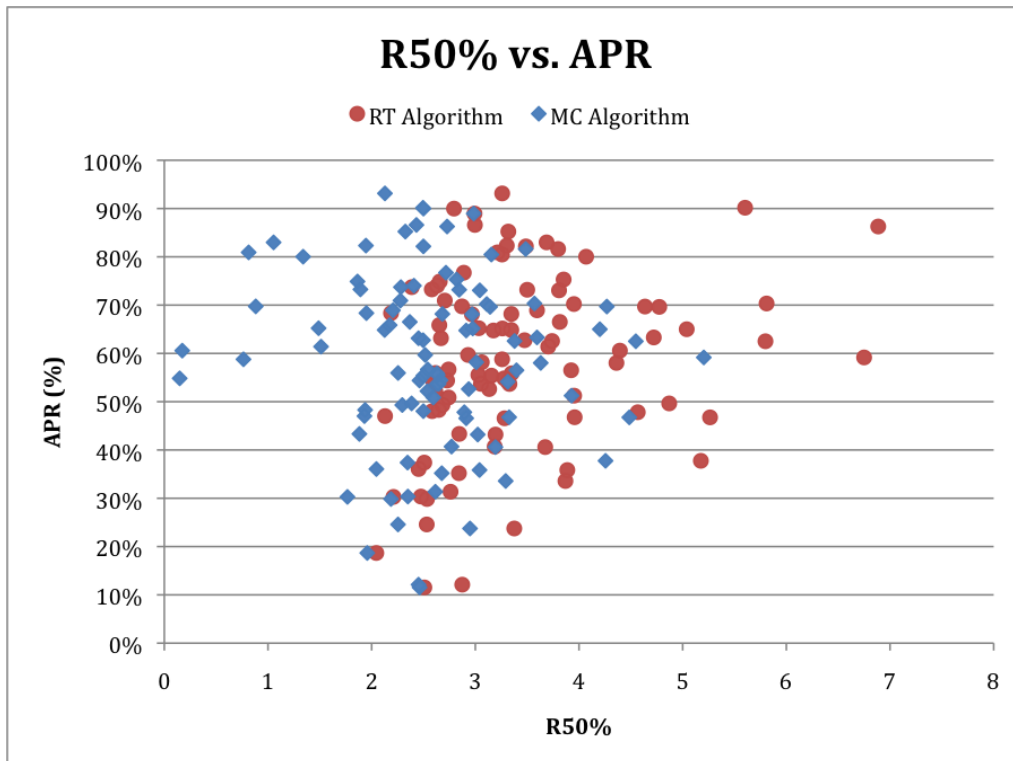


Figure 26: RTOG Protocols: R50% versus APR.

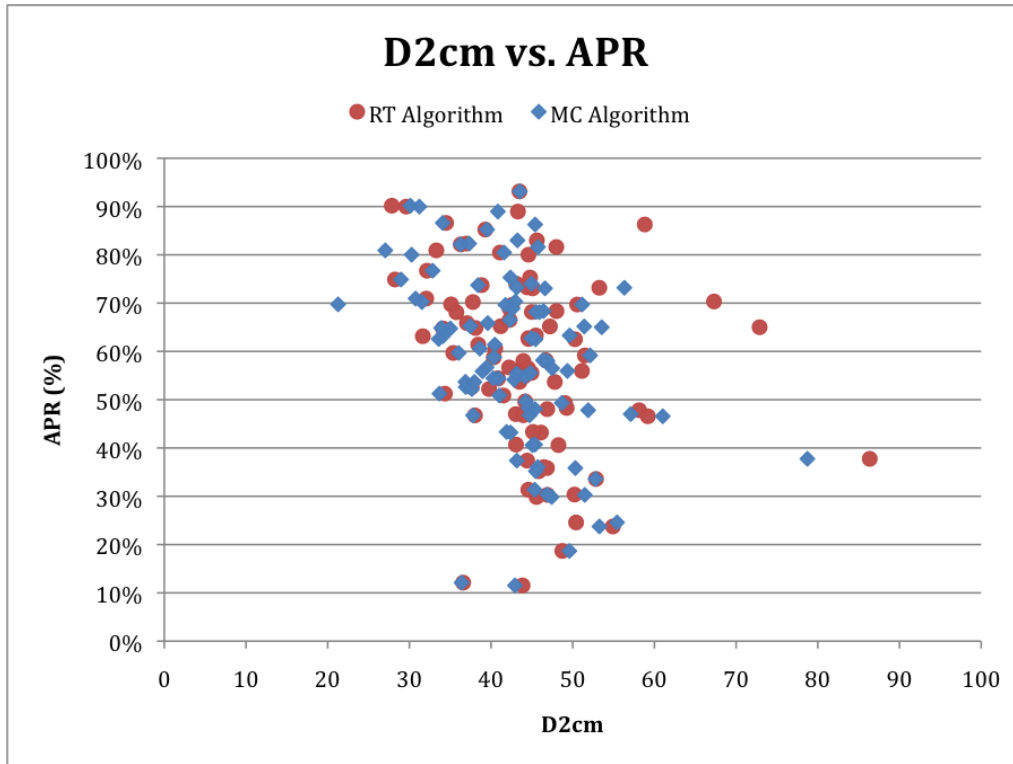


Figure 27: RTOG Protocols: D2cm versus APR.

The normalized differences (expressed as percent change) for the individual plans between the RT and MC calculated RTOG parameters were also calculated. The correlation coefficients for these differences compared with both the PTV volume and the APR are included in Table VIII as well. The correlation coefficient of the CI difference with the PTV is 0.35 and for the R50% difference is 0.34. The correlation coefficients for those same parameters compared with APR are 0.43 and 0.31, respectively.

D. Organs at Risk (OAR)

Normalized mean differences, expressed as a percent change from RT to MC, and standard deviations for the OAR are given in Table IX. Maximum doses (Dmax) delivered to OARs were reduced in the MC plans: reduction of maximum dose for the

spinal cord 18.1%, esophagus was 13.3%, heart 12.8%, great vessels 10.1%, trachea and ipsilateral main bronchus 16.5%, and ribs 9.8%. The volume of the total lung minus PTV was between 30-32% lower for MC at 5, 10, and 20Gy points. The doses for 1000 and 1500 cc of total lung minus PTV, respectively were reduced by 36.1% and 47.8% for the MC plan. The standard deviations indicate that the variability from plan to plan is large for most of these OARs, especially for the Dmax heart (standard deviation is 31.7), Dmax trachea and ipsilateral main bronchus (23.7), and for the dose for 1500cc and 1000cc of total lung minus PTV (28.4 and 29.2, respectively). Figure 28 shows the change in Dmax (in 30 mm³ of volume) for several OAR and plus or minus the standard deviation as an error bar for each.

Table IX: OAR Data Details.

| Organ at Risk | Number of Cases | (MC – RT) / RT (%) | Standard Deviation of Normalized Mean |
|--|-----------------|--------------------|---------------------------------------|
| Dmax Spinal Cord | 102 | -18.1 | 15.1 |
| Dmax Esophagus | 102 | -13.3 | 12.0 |
| Dose for 5 cc of Esophagus | 102 | -24.0 | 19.0 |
| Dmax Heart | 102 | -12.8 | 31.7 |
| Dose for 15 cc of Heart | 102 | -23.7 | 24.2 |
| Dmax Great Vessels | 97 | -10.1 | 16.1 |
| Dmax Trachea and Ipsilateral Main Bronchus | 92 | -16.5 | 23.7 |
| Dmax Ribs | 20 | -9.8 | 12.7 |
| Volume Total Lungs – PTV at 500cGy | 102 | -30.3 | 16.9 |
| Volume Total Lungs – PTV at 1000cGy | 102 | -30.5 | 18.0 |
| Volume Total Lungs – PTV at 2000cGy | 99 | -32.0 | 19.2 |
| Dose for 1500cc of Total Lung – PTV | 97 | -47.8 | 28.4 |
| Dose for 1000cc of Total Lung – PTV | 102 | -36.1 | 29.2 |

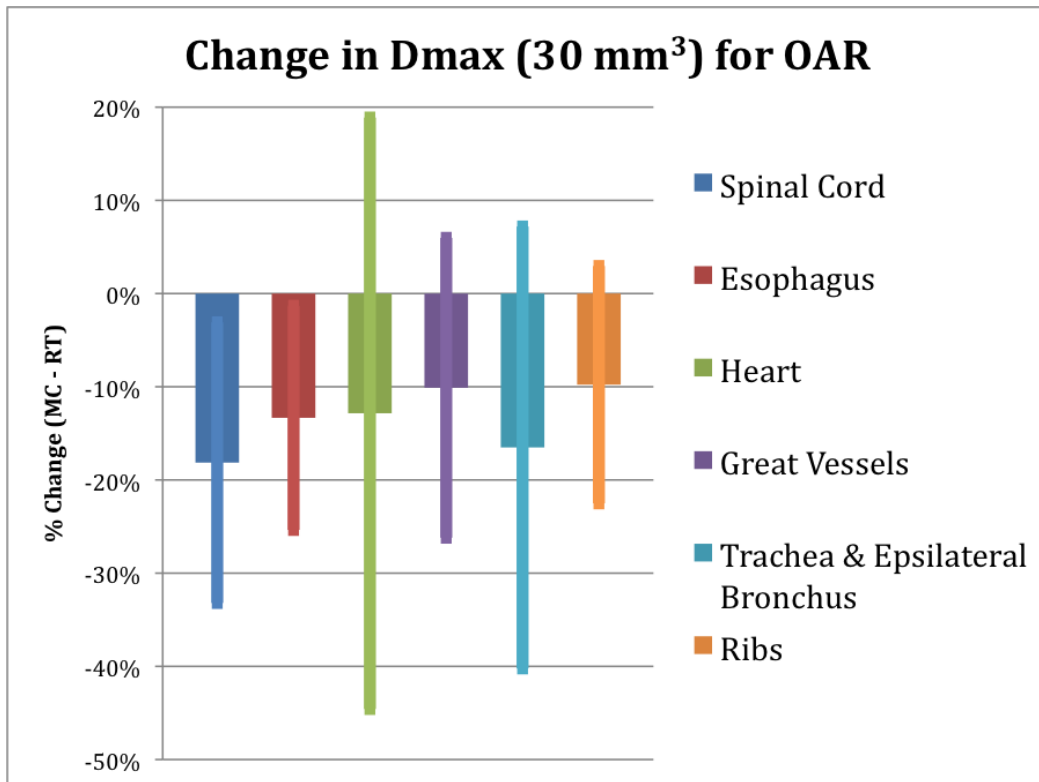


Figure 28: Change in Dmax (30mm³) for OAR. Also included are error bars for +/- 1 standard deviation.

IV. CONCLUSIONS

The presented results indicate that there are significant differences between the dose plans calculated using the RT algorithm and those calculated using the MC algorithm, with the RT algorithm consistently overestimating doses. These overestimates are largest for small PTV and/or when the ratio of the volume of lung tissue to the PTV (APR) approaches 1.

The lower dose parameters for both GTV and PTV for the MC calculated plans could be described as a shift in the DVH curve toward lower doses for both GTV and PTV and the results suggest this shift is most pronounced for the top of the curve (including dose parameters Dmax, D99, and D95). The changes for individual plans are moderately correlated with both GTV and PTV, but the variability for individual plans is high indicating a direct linear correction to the RT calculated plans is not possible. This strongly suggests a re-optimization of the MC algorithm plans is necessary for all plans. By comparing the individual plan changes to APR, the dose parameter correlations are found to increase slightly, suggesting any correction should include this parameter.

The biological equivalent dose (BED) results also indicate that the RT plans are overestimating calculated doses. The normalized difference between the BED means calculated for the two algorithms showed a decrease in calculated dose from the RT

algorithm to the MC algorithm and this overestimation was shown to be a function of APR, with larger differences occurring when the APR was closer to 1.

The difference for the RTOG protocol parameters between the two algorithms was greatest for the CI. For this parameter, not only was there a shift from the RT algorithm to the MC algorithm, but when the individual plan differences were plotted versus APR, the CI values for MC showed a relationship between the CI and APR that was not apparent when the RT CI values were plotted. This provides further evidence that the APR should be used for any correction between the two algorithms. All OARs showed a mean shift toward lower doses for the MC calculated plans versus the RT calculated plans, though for some individual plans, the doses were higher when using the MC algorithm.

The AAPM task group #105 reported that “dose differences as low as 5-10% are reported to be clinically detectable, and may result in 10-20% in tumor control probability or 20-30% normal tissue complication probability.”^{xxiii, xxiii} As a consequence, MC calculation and optimization for all lung cancer treatment plans should be required as standard of care. The results in the current study support this conclusion, especially with regard to cases when the APR is large.

APPENDICES

A. Appendix 1: IRB Letter



Institutional Review Board - Human Research Protections

Broward Health Medical Center
Broward Health Coral Springs
Broward Health Imperial Point
Broward Health North
Chris Evert Children's Hospital
Broward Health Weston
Community Health Services
Broward Health Physician Group

January 20, 2014

Raj Selvaraj M.S., DABR
Pennington, Andreea
BHNNorth-21 Century Oncology
201 E. Sample Road
Deerfield Beach FL 33064-

Internal # 4904

Protocol Title: EXEMPT: Comparison of Treatment Plans Calculated Using Ray Tracing and Monte Carlo Algorithms for Lung Patients Having Undergone Radiotherapy with Cyberknife. 01/20/2014.

Approval Date: 01/20/2014
Study Expiration: 10/19/2014

Dear Mr. Selvaraj:

The Broward Health's Institutional Review Board has conducted a review of the above referenced project. It was determined this project is considered non-research related activities. Based on its findings the above project was granted an exempt status.

The next review for this project will be due on or before 10/19/2014. If it is necessary to continue this project beyond this date, a request for continuation of this project must be submitted prior to the expiration of this study.

Project Expiration: 10/19/2014

Sponsor/ School: Florida Atlantic University
Master Thesis

Reason: Request Project Exempt Status
Description: * Research Project Exempt application
* Department letter of support
* Protocol design
* CV/ licenses
* Other related documents

Facility/ Dept: BH North 21 Century Radiation Oncology

Risk Analysis: The IRB has determined this project does not involve greater than minimal risk. This project include written assurance that Protected Health Information will not be re-used or disclosed to any other entity outside Broward Health's Institution for any purpose other than approved by the IRB as required by law.

Exempt Status: 45 CFR 46.101(b)(4) Research involving the collection of existing data (secondary)

Action: Exempted

All research activities including data collection is prohibited after expiration 10/19/2014 unless continued renewal of this study is granted by the IRB.

It is the responsibility of the principal investigator to communicate protocol progress, closures, and/or terminations in accordance with the Code of Federal Regulations. The information contained herein is true and correct as reflected in the records of Broward Health Institutional Review Board (IRB). This institutional review board operates in accordance with the Office of Human Research Protections and Good Clinical Practices (GCP) under the U.S. Food and Drug Administration (FDA) regulations.

Sincerely,

A handwritten signature in black ink, appearing to read "Robin M. Smith".

Robin M. Smith, MBA, CIM, CIP
Broward Health Institutional Review Board
FWA00001248

REFERENCES

-
- ⁱ Schottenfeld, D. (2010). The Etiology and Epidemiology of Lung Cancer. In Pass, H. I. et al. (Eds.). *Principles and practice of lung cancer: the official reference text of the IASLC* 4th Ed (pp. 1-46). Philadelphia: Lippincott Williams & Wilkins.
- ⁱⁱ WHO Fact Sheet No. 297. (2012). *Cancer*. Retrieved from <http://www.who.int/mediacentre/factsheets/fs297/en/>
- ⁱⁱⁱ Grills, I. S. and Mangona, V.S. (2011). Intensity-Modulated Radiation Therapy and Volumetric-Modulated Arc Therapy for Lung Cancer. In Jeremic, B. (Ed.). *Advances in Radiation Oncology in Lung Cancer* 2nd Ed. (pp. 691-762). Berlin: Springer-Verlag.
- ^{iv} Wilcox, E. E. et al. (2010). Comparison of planned dose distributions calculated by Monte Carlo and Ray-Trace algorithms for the treatment of lung tumors with CyberKnife: A preliminary study in 33 patients. *International Journal of Radiation Oncology, Biology & Physics*, 77(1), 277-284.
- ^v Dela, C. C. S., Tanoue, L. T. and Matthay, R. A. (2011). Lung cancer: Epidemiology, etiology, and prevention. *Clinics in Chest Medicine*, 32(4), 605-44.
- ^{vi} Samet, J. M., Humble, C. G. and Pathak, D. R. (1986). Personal and family history of respiratory disease and lung cancer risk. *Am Rev Respir Dis*, 134, 466–470.

-
- ^{vii} Larsen, J. E. et al. (2010). An Overview of the Molecular Biology of Lung Cancer. In Pass, H. I. et al. (Eds.). *Principles and practice of lung cancer: the official reference text of the IASLC* 4th Ed (pp. 59-74). Philadelphia: Lippincott Williams & Wilkins.
- ^{viii} Kameyama, K. et al. (2009). Evaluation of the new TNM staging system proposed by the International Association for the Study of Lung Cancer at a single institution. *J Thorac Cardiovasc Surg*, 137(5), 1180-1184.
- ^{ix} Achen, M. A. and Stacker, S. A. (2008). Molecular Control of Lymphatic Metastasis. *Ann. N.Y. Acad. Sci.*, 1131, 225–234.
- ^x Kong, F. M. et al. (2011). Consideration of dose limits for organs at risk of thoracic radiotherapy: atlas for lung, proximal bronchial tree, esophagus, spinal cord, ribs, and brachial plexus. *Int. J. Radiation Oncology Biol. Phys.*, 81(5), 1442–1457.
- ^{xi} Stewart, A. J. and Jones, B. (2007). Radiobiologic Concepts for Brachytherapy. In Devlin, P. M. (Ed.). *Brachytherapy: Applications and Technique*, 1st Ed (pp. 1-19). Philadelphia: Lippincott Williams & Wilkins.
- ^{xii} Slate, L. J. et al. (2004). A Monte Carlo Brachytherapy Study for Dose Distribution Prediction in in Inhomogeneous Medium. *Medical Dosimetry*, 29(4), 271-278.
- ^{xiii} ICRU 38. (1985). *Dose and volume specifications for reporting intracavitary therapy in gynecology*. Bethesda, MD: International Commission on Radiation Units and Measurements.

-
- ^{xiv} Suntharalingam, N., Podgorsak, E. B. and Tolli, H. (2005). Brachytherapy: Physical And Clinical Aspects. In Podgorsak, E. B. (Ed.). *Radiation Oncology Physics: A Handbook for Teachers and Students* (pp. 451-484). Vienna: International Atomic Energy Agency.
- ^{xv} Hoskin, P. and Coyle, C. (2012). *Radiotherapy in Practice – Brachytherapy*, 2nd Ed. Oxford: Oxford University Press.
- ^{xvi} Johns, H. E. and Cunningham, J. R. (1983). *The physics of radiology*, 4th Ed. Illinois: Charles C. Thomas Publishers.
- ^{xvii} Saito, S., Nagata, H., Kosugi, M., Toya, K. and Yorozu, A. (2007). Brachytherapy with permanent seed implantation. *International Journal of Clinical Oncology*, 12(6), 395-407.
- ^{xviii} Miften, M. M., Beavis, A. W. and Marks, L. B. (2002). Influence of Dose Calculation Model on Treatment Plan Evaluation in Conformal Radiotherapy: A Three-Case Study. *Medical Dosimetry*, 27(1), 51–57.
- ^{xix} Martel, M. K. (2011). 3D Radiation Treatment Planning and Execution. In Jeremic, B. (Ed.). *Advances in Radiation Oncology in Lung Cancer* 2nd Ed. (pp. 143-156). Berlin: Springer-Verlag.
- ^{xx} Renaud, J., Yartsev, S., Dar, A. R. and Dyk, J. V. (2009). Adaptive Radiation Therapy for Localized Mesothelioma with Mediastinal Metastasis Using Helical Tomotherapy. *Medical Dosimetry*, 34(3), 233-242.

-
- ^{xxi} Webb, S. (2005). *Contemporary IMRT: Developing Physics and Clinical Implementation*. London: IOP Publishing Ltd.
- ^{xxii} Chen, Q., Chen, M. and Lu, W. (2011). Ultrafast convolution/superposition using tabulated and exponential kernels on GPU. *Med. Phys.*, 38(3), 1150-1161.
- ^{xxiii} Chetty, I. et al. (2007). Report of the AAPM Task Group No. 105: Issues associated with clinical implementation of Monte Carlo-based photon and electron external beam treatment planning. *Med. Phys.*, 34(12), 4818-4853.
- ^{xxiv} Alber, M. et al. (2008). Guidelines for the verification of IMRT. *Estro Booklet No. 9*. Brussels: Estro.
- ^{xxv} Cherry, S. R., Sorenson, J. and Phelps, M. (2012). *Physics in Nuclear Medicine* 4rd Ed. Philadelphia: Saunders.
- ^{xxvi} Mettler, F. A. and Guiberteau, M. J. (2006). *Essentials of Nuclear Medicine Imaging*. Pennsylvania: Saunders Elsevier.
- ^{xxvii} Rahmim, A. and Zaidi, H. (2008). PET versus SPECT: strengths, limitations and challenges. *Nuclear Medicine Communications*, 29(3), 193-207.
- ^{xxviii} Palma, D. A., Verbakel, W. F., Otto, K. and Senan, S. (2010). New developments in arc radiation therapy: A review. *Cancer Treat Rev.* 36, 393–399.
- ^{xxix} Van Esch, A. et al. (2011). Implementing RapidArc into clinical routine: A comprehensive program from machine QA to TPS validation and patient QA. *Med. Phys.*, 38(9), 5146-5166.

-
- ^{xxx} Seppala, J., Suilamo, S., Kulmala, J., Mali, P. and Minn, H. (2012). A dosimetric phantom study of dose accuracy and build-up effects using IMRT and RapidArc in stereotactic irradiation of lung tumours. *Radiation Oncology*, 7, 79-89.
- ^{xxxi} Ong, C. L., Cuijpers, J. P., Senan, S., Slotman, B. J. and Verbakel, W. F. A. R. (2011). Impact of the calculation resolution of AAA for small fields and RapidArc treatment plans. *Med. Phys.* 38(8), 4471-4479.
- ^{xxxii} Ho, A. K., Gibbs, I. C., Chang, S. D., Main, B. and Adler, J. R. (2008). The Use of TLD and Gafchromic Film to Assure Submillimeter Accuracy for Image-Guided Radiosurgery. *Medical Dosimetry*, 33(1), 36-41.
- ^{xxxiii} Ma, C. M., Li, J. S., Deng, J. and Fan, J. (2008). Implementation of Monte Carlo Dose Calculation for CyberKnife treatment planning. *Journal of Physics: Conference Series* 102(1), 1-10.
- ^{xxxiv} Accuray CyberKnife Equipment Specifications. (2009). California: Accuray Incorporated. Retrieved from: <http://www.cyberknifelatin.com/pdf/brochure-tecnico.pdf>
- ^{xxxv} Nuytens, J. J. and Bondiau, P. Y. (2012). Role of 4D Stereotactic Radiotherapy with the CyberKnife® System in the Treatment of Lung Cancer. Retrieved from <http://www.touchoncology.com/system/files/private/articles/19818/pdf/nuytensfinalepub.pdf>
- ^{xxxvi} Zyp, N. C. et al. (2009). Stereotactic radiotherapy with real-time tumor tracking for non-small cell lung cancer: Clinical outcome. *Radiotherapy and Oncology*, 91, 296–300.

^{xxxvii} Benedict, S. H. et al. (2010). Stereotactic body radiation therapy: The report of AAPM Task Group 101. *Med. Phys.* 37(8), 4078-4101.

^{xxxviii} Guckenberger, M. et al. (2007). Precision of image-guided radiotherapy IGRT in six degrees of freedom and limitations in clinical practice. *Strahlenther Onkol.*, 183(6), 307–313.

^{xxxix} Meyer, J. L. (Ed.) (2007). *IMRT, IGRT, SBRT: Advances in the Treatment Planning and Delivery of Radiotherapy*. Basel: S. Karger Ag.

^{xl} Timmerman, R. et al (2010). Stereotactic Body Radiation Therapy for Inoperable Early Stage Lung Cancer. *The Journal of the American Medical Association*, 303(11), 1070-1076.

^{xli} Michalski, J. et al. (2004). *A Phase II Trial of Stereotactic Body Radiation Therapy (SBRT) in the Treatment of Patients with Medically Inoperable Stage I/II Non-Small Cell Lung Cancer*. RTOG 0236.

^{xlii} Timmerman, R. et al. (2010). *A Phase II Trial of Stereotactic Body Radiation Therapy (SBRT) in the Treatment of Patients with Operable Stage I/II Non-Small Cell Lung Cancer*. RTOG 0618.

^{xliii} Bezjak, A. et al. (2010). *Seamless Phase I/II Study of Stereotactic Lung Radiotherapy (SBRT) for Early Stage, Centrally Located, Non-Small Cell Lung Cancer (NSCLC) in Medically Inoperable Patients*. RTOG 0813.

^{xliv} Ryu, S. et al. (2011). *Phase II/III Study of Image-Guided Radiosurgery/SBRT for Localized Spine Metastasis*. RTOG 0631.

^{xliv} Sharma, S. C., Ott, J. T., Williams, J. B. and Dickow, D. (2009). Clinical implications of adopting Monte Carlo treatment planning for CyberKnife. *Journal of Applied Clinical Medical Physics*, 11(1), 170-175.

^{xlvi} Zyp, N. C. et al. (2010). Clinical introduction of Monte Carlo treatment planning: A different prescription dose for non-small cell lung cancer according to tumor location and size. *Radiotherapy and Oncology*, 96, 55–60.

^{xlvi} CyberKnife Whitepaper. (2010). Monte Carlo Dose Calculation Algorithm for the Cyberknife® Robotic Radio Surgery System. California: Accuray Incorporated.
Retrieved from http://www.cyberknife.com.tr/images/yayin/MonteCarlo_Whitepaper.pdf

^{xlvi} Ma, C. M., Li, J. S., Pawlicki, P., Jiang, S. B., Deng, J. et al. (2004). MCSIM: A Monte Carlo dose calculation tool for radiation therapy, In Yi, B. Y. et al. (Eds.) *Proc. of the 14th International Conference on the Use of Computer in Radiation Therapy (ICCR)* (pp. 515-519). Seoul: Jeong Publishing.

^{xlvi} Frey, E. C. and Tsui, B. M. W. (2006). Collimator-Detector Response Compensation in SPECT. In Zaidi, H. (Ed.), *Quantitative Analysis in Nuclear Medicine Imaging* (pp. 141-166). New York: Springer.

ⁱ AAPM Report No. 85, 2004, p. 35.

-
- ^{li} Papanikolaou, N. and Stathakis, S. Dose-calculation algorithms in the context of inhomogeneity corrections for high energy photon beams. *Med. Phys.*, 36(10), 4765-4775.
- ^{lii} Fotina, I. et al. (2011). Clinical comparison of dose calculation using the enhanced collapsed cone algorithm vs. a new Monte Carlo algorithm *Strahlenther Onkol*, 187 433–441.
- ^{liii} Streit, R. L. (2010). *Poisson Point Processes: Imaging, Tracking, and Sensing*. New York: Springer.
- ^{liv} Block, B., Virnau, P. and Preis, T. (2010). Multi-GPU accelerated multi-spin Monte Carlo simulations of the 2D Ising model. *Computer Physics Communications*, 181, 1549–1556.
- ^{lv} DeMarco, J. J., Chetty, I. J. and Solberg, T. D. (2002). A Monte Carlo Tutorial and the Application for Radiotherapy Treatment Planning. *Medical Dosimetry*, 27(1), 43–50.
- ^{lvi} Salvat, F., Fernández-Varea, J. M. and Sempau, J. (2008). *PENELOPE-2008: A code system for monte carlo simulation of electron and photon transport*. Issy-les-Moulineaux: OECD Nuclear Energy Agency. Retrieved from <http://www.oecd-neo.org/science/pubs/2009/nea6416-penelope.pdf>
- ^{lvii} Grofsmid, D. et al. (2010). Dosimetric validation of a commercial Monte Carlo based IMRT planning system. *Med. Phys.*, 37(2), 540-549.

-
- ^{lviii} Bush, K. et al. (2011). Dosimetric validation of Acuros® XB with Monte Carlo methods for photon dose calculations. *Med. Phys.*, 38(4), 2208-2221.
- ^{lix} Taylor, M. et al. (2012). Determination of peripheral underdosage at the lung-tumor interface using Monte Carlo radiation transport calculations. *Medical Dosimetry*, 37(1), 61-66.
- ^{lx} Ahn, Y. C. (2014). Role of Radiation Therapy for Non-small Cell Lung Cancer: Focused on Stereotactic Ablative Radiation Therapy in Stage I. *Hanyang Medical Review*, 34(1), 45-50.
- ^{lxi} ICRU 62. (1999). *Prescribing, Recording and Reporting Photon Beam Therapy (Supplement to ICRU Report 50)*, ICRU Report 62. Bethesda, MD: International Commission on Radiation Units and Measurements.
- ^{lxii} Miura, H. et al. (2014). Clinical Introduction of Monte Carlo Treatment Planning for Lung Stereotactic Body Radiotherapy. *Journal of Applied Clinical Medical Physics*, 15(1), 38-43.
- ^{lxiii} Ojala, J. et al. (2014). Performance of Dose Calculation Algorithms from Three Generations in Lung SBRT: Comparison with Full Monte Carlo-based Dose Distributions. *Journal of Applied Clinical Medical Physics*, 15(2), 4-18.